SPATIAL CONTROL OF CAVITATION IN THERAPEUTIC ULTRASOUND

by

Thomas P. Gauthier

Submitted to the Department of Electrical Engineering and Computer Science
in Partial Fulfillment of the Requirements for the Degree of

MASTER OF SCIENCE IN ELECTRICAL ENGINEERING
AND COMPUTER SCIENCE

at the

MASSACHUSETTS INSTITUTE OF TECHNOLOGY

February 2005

Signature of Author_____

Thomas P. Gauthier
Department of Electrical Engineering and Computer Science
December 10, 2004

Certified by_____

Kullervo Hynynen, PhD
Professor of Radiology, Harvard Medical School
Thesis Advisor

Certified by_____

H. Frederick Bowman, PhD
Senior Academic Administrator, Harvard-MIT
Division of Health Sciences & Technology
Departmental Advisor

Accepted by_____

Arthur C. Smith, PhD
Chairman, Committee on Graduate Students
Department of Electrical Engineering and Computer Science

Spatial Control of Cavitation in Therapeutic Ultrasound

by
Thomas P. Gauthier

Submitted to the Department of Electrical Engineering and Computer Science
in Partial Fulfillment of the Requirements for the Degree of
Master of Science in Electrical Engineering and Computer Science
at the
Massachusetts Institute of Technology
February 2005

Abstract

Inertial cavitation has been implicated as the primary mechanism for a host of emerging applications. In all these applications, the main concern is to induce cavitation in perfectly controlled locations in the field; this means specifically to be able to achieve cavitation threshold at the geometrical focus of the transducer without stimulating its near field. In this study, we make use of dual-frequency methods to preferentially lower the cavitation threshold at the focus relative to the rest of the field. One family of dual-frequency driving waveforms is evaluated in a bubble model incorporating rectified diffusion. Theoretical predictions based on Sokka's work (Sokka 2003a) are confirmed *in vitro* using Optison™, a commercially available contrast agent. The performance of the rest of acoustic field in suppressing cavitation when cavitation is induced at the focus is investigated theoretically and checked experimentally. This first part shows that dual-frequency phased arrays could be used to precisely control cavitation. Cavitation threshold is proved to be 1.2 times higher in the near field than at the focus.

One of the main limitations of the aforementioned protocol is that it is tightly controlled. As an example, Optison™ has a mean bubble size of 2 - 4.5 μm, which means that the initial bubble radii will fall in this range. Since cavitation threshold has been proved to depend on this parameter, using ultrasound contrast agents allows for more predictable results. Therefore, in the second half of this study, we propose a focused ultrasound protocol that induces and monitors gas bubbles at the focus and allows for *ex vivo* validation of the aforementioned theoretical results. The experiments involve fresh rabbit tissue and a statistical analysis is performed over data collected from back muscle. Moreover, the experimental apparatus is designed to be MRI-compatible to make future *in vivo* assessments feasible. This second half of the study demonstrates that the theoretical predictions made earlier can reliably be used to predict dual-frequency cavitation thresholds. It also suggests that clinical use of dual-frequency excitations might be a solution to the problem of spatial control of cavitation.

Thesis Advisor: Kullervo Hynynen, PhD
Title: Professor of Radiology, Harvard Medical School and Brigham and Women's Hospital

ACKNOWLEDGMENTS

I would like to thank Professor Kullervo Hynynen for the opportunity to work on this project and for providing an ideal environment for research. I would also like to thank other members of the research group at the Brigham and Women's Hospital: Dr. Greg Clement, Dr. Nathan McDannold, Jason White, Danish Khatri, Jose Juste, and Erich Caulfield.

I would also like to thank all those people who facilitated my entrance in the ultrasound world. I would especially like to thank Professor Mathias Fink, Dr. Mickael Tanter, and Aline Criton.

Most importantly, I would like to thank my family for unconditional support and love. Many thanks to my parents, papi et mamie Nini, my sister Marianne, and of course my wife Marion. I would also like to dedicate this thesis to papi et mamie Arsène, as they won't be able to attend the Commencement ceremony but would certainly be proud of their little *Tommy*.

TABLE OF CONTENTS

List of figures

List of tables

1. Introduction

1.1. Background

1.1.1. Focused Ultrasound Surgery

Focused Ultrasound Surgery (FUS) is defined as the use of focused ultrasound to coagulate tissue. It has been extensively investigated and found to provide an efficient way to treat benign and cancerous tumors in several organs systems (Hynynen *et al* 1996a, Vallancien 1996).

When used in the therapeutic frequencies range, 0.5 to 4 *MHz*, ultrasound can be tightly focused (on the order of the wavelength) with very little power deposition in the near field. As an example, a sinusoidal ultrasound wave at 1.0 *MHz* has a wavelength of 1.5 mm and a penetration depth of roughly 10 cm in soft tissue (Hynynen and Lulu 1990). In comparison, a microwave, which radiates at 2450 *MHz* has a wavelength of 1.8 cm and a penetration depth of only 1.7 cm in tissue (Johnson 1972). These specifications therefore allow ultrasound transducers to be extracorporeal devices for noninvasive treatment. Ultrasound can cause tissue necrosis via two methods: *1.* energy absorption resulting in temperature elevation and *2.* the implosion of cavitating bubbles induced by higher pressure ultrasound waves.

Up to now, researchers have tried to avoid cavitation and always used the thermal mode in FUS treatments as it is better characterized and controlled, yielding lesion sizes and shapes predicted by models (Carstensen *et al* 1981, Damianou *et al* 1995, Hill *et al* 1994, Lizzi and Ostromogilsky 1987). FUS thermal ablation is performed with constant levels of ultrasound intensity well below the cavitation threshold for durations of 1-30 seconds ensuring that the temperature at the focus reaches levels that denature protein causing tissue necrosis. In addition, therapy in the thermal regime can be carefully monitored with thermometry techniques most notably MRI. MRI provides excellent soft tissue contrast for diseased tissue segmentation. Moreover, temperature sensitive pulse sequences can be used to measure relative temperature changes (Chung *et al* 1996, Ishihara *et al* 1995, Samulski *et al* 1992). Several studies have shown the feasibility of MRI-guided ultrasound surgery *in vivo* (Cline *et al* 1995, Hynynen *et al* 1996b, Hynynen

et al 1993, McDannold *et al* 1998, Stepanow *et al* 1995). More recent work has shown that MRI thermal dosimetry techniques can be used to accurately predict the extent of thermal tissue damage (Chung *et al* 1999, Hazle *et al* 2002, McDannold *et al* 2001).

1.1.2. Cavitation

Acoustic cavitation is defined as any observable activity involving a gas bubble stimulated into motion by an exposure to an acoustic field. It has been extensively studied and is divided in two basic types: *1.* stable and *2.* inertial cavitation (Duck 1998). Stable cavitation is the less violent event and refers to radial oscillations of gas bubbles without collapse; these radial oscillations may be nonlinear (Leighton 1994). When entering inertial or transient cavitation regime, bubbles can grow to twice their initial bubble size (meaning that their radius grows to twice their initial value) and then have sufficient energy in order to violently collapse. When cavitation is initiated *in vivo*, a series of bioeffects can occur. For example, shock waves may be propagated, acoustic energy is often converted to heat yielding high microscopic temperatures (1000-20,000 ^{o}K) (Flynn 1982). One very important feature of inertial cavitation is that it is a threshold phenomenon. When sonicating in a specific medium, there will be a threshold ultrasound intensity above which inertial cavitation will occur. This intensity threshold is not only varying from a given tissue to another, but it is also frequency-dependent. Cavitation thresholds *in vivo* have been studied yielding variable intensity values in different tissues at different frequencies (Hynynen 1991, Lele 1977, Prat *et al* 1994, Sanghvi 1998). Many intricate physical principles actually govern the dynamics of gas bubbles when stimulated by an acoustic pressure field. A rigorous model of bubble inception, growth, and collapse would require integrating all of them.

Inducing cavitation in a medium first requires bubbles to seed. In order to form a cavity in a liquid, sufficient tension is required to pull apart the liquid (Leighton 1994). When a liquid is sonicated by ultrasound, negative pressures, pressures below the ambient pressure, can put the liquid in tension. Several different factors can essentially seed bubbles and act to lower the tension required for bubble formation and cavitation. Impurities in the liquid, the presence of dissolved gas, preexisting cavities, or crevices in

the surfaces of the liquid container can all play such a role. Once the process of seeding is achieved, these bubbles may dissolve, grow, collapse or oscillate in a pressure field. If the bubbles are not insonified by an ultrasound field, they typically tend to dissolve due to surface tension. This is especially true for smaller bubbles as surface tension varies inversely with the radius of the bubble. When now in the presence of an acoustic field, the behavior of these bubbles is completely modified. To model the behavior of a single bubble in an acoustic pressure field, we may first assume this bubble to act as a driven harmonic oscillator. In this model, the gas features would provide the stiffness while the surrounding liquid would supply the inertia. A first refinement of this model could consist in incorporating first-order viscous damping by adding a damping term. The harmonic oscillator model is especially useful in order to describe stable cavitation. It is also helpful to calculate resonance frequency given the initial bubble radius. This frequency is known as the Minnaert resonance frequency. For air bubbles in water at 1 atmosphere, the resonance frequency simplifies to $3\ m.s^{-1} / R_o$, where R_0 is the equilibrium or initial bubble radius. Since the bubble is essentially a nonlinear oscillator, the harmonic oscillator model might just be useful to provide an initial guess of the resonance frequency. Several researchers have built up nonlinear models which are better suited to take care of the bubble's inherent nonlinear behavior. Most of these models are based on the Rayleigh-Plesset equation which models a single bubble in an infinite incompressible medium. Moreover, this equation assumes that the bubble motion is spherically symmetric. The Rayleigh-Plesset equation is shown below with R as the time-varying bubble radius, ρ as the density, σ as the surface tension, η as the shear viscosity, κ as the polytropic index, R_0 as the initial bubble radius, p_v as the vapor pressure, p_0 as the ambient pressure, and $P(t)$ as the time-varying pressure field at the bubble.

$$R\ddot{R} + \tfrac{3}{2}\dot{R}^2 = \frac{1}{\rho}\left\{\left(p_0 + \frac{2\sigma}{R_0} - p_v\right)\left(\frac{R_0}{R}\right)^{3\kappa} + p_v - \frac{2\sigma}{R_0} - \frac{4\eta\dot{R}}{R} - p_0 - P(t)\right\}$$

Even though the Rayleigh-Plesset equation takes into account the inherent nonlinear behavior of a bubble, it still has some serious limitations. First of all, it doesn't incorporate liquid incompressibility. Therefore the model is not able to completely

describe violent bubble collapse. Compressibility has been added to this model by various mechanisms (Flynn 1964, Flynn 1975, Gilmore 1952, Keller and Miksis 1980, Kirkwood and Bethe 1942, Prosperetti *et al* 1988), and associated results have been validated by experiment (Gaitan *et al* 1992).

Even though these equations are not very representative of bubble activity in tissue, they can still be used to make predictions of cavitation inception and cavitation thresholds *in vivo*. In tissues, bubble activity involves bubble clouds and various bubble stabilizing agents. In addition, the aforementioned models assume that the liquid is a Newtonian fluid; unfortunately, tissue is generally non-Newtonian. These models also closely depend on initial bubble radii and gas concentrations; in tissue environments, these parameters are not easily accessible. Despite the above limitations, these bubble models can be used to extract general trends on cavitation thresholds and bubble responses to various acoustic pressures. One of these non-linear models was used to predict cavitation thresholds *in vivo*; it has theoretically showed the dependence of inertial cavitation threshold on frequency, initial bubble radii, and local gas concentration (Apfel 1981). At a high enough temperature, bubbles acquire sufficient energy for violent collapse. The gas temperature versus time can be computed from the time-varying bubble radius with some assumptions on the nature of the gas, and therefore the pressures required for cavitation can be predicted. As an alternative, Noltingk and Neppiras proposed that transient or inertial cavitation threshold is reached when $\frac{R}{R_0} \approx 2$ for biomedical frequencies of ultrasound. This was later confirmed by Flynn (Flynn 1975).

Another serious limitation of the discussed bubble models is to ignore another important factor which can contribute to bubble growth in tissue. Termed rectified diffusion, Harvey *et al* observed that in animals, bubbles in oscillation exhibit a steady increase in R_0 during a sustained insonation. The inward diffusion of gas arises from the fall of internal bubble pressure during the bubble expansion phase setting up a pressure gradient. Two specific mechanisms are known to increase the rectified diffusion capacity, the area effect and the shell effect (Leighton 1994). In the area effect, the increased bubble size during the expansion phase provides more surface area for gas diffusion. With shell effect, the liquid shell around the gas bubble gets thinner during expansion

increasing the diffusion gradient across the bubble wall. These effects have been theoretically modeled (Crum 1980, Eller 1969, Lewin and Bjorno 1981). Church has the most sophisticated model, in which, he computes the time varying bubble radius and then uses this radius to predict the rectified diffusion rate. He then determines the minimum pressure required to induce bubble growth by rectified diffusion, the rectified diffusion threshold. Once the threshold is reached, the bubble grows larger during every negative pressure cycle ultimately reaching a size when violent collapse can occur. Although he concludes that rectified diffusion does not occur at ultrasound imaging frequencies and pressures, pressure waveforms may be designed to reduce the rectified diffusion threshold to induce rectified diffusion and subsequent cavitation.

At the present time, cavitation and its associated effects *in vivo* can't be fully characterized. However, general trends in cavitation and its thresholds *in vivo* can be extracted from currently used bubble models. These models could further be used to design optimal cavitation therapies.

1.1.3. Cavitation in therapeutic ultrasound

The prospect of *in vivo* acoustic cavitation was first described in frogs in 1950 (Fry *et al* 1950). This work was soon followed by Lehmann (Lehmann and Herrich 1953) who proved that *in vivo* cavitation was potentially the cause of observable blood vessel damage at 1 *MHz* at some unknown high intensity. The use of focused ultrasound for central nervous tissue destruction was further studied; moreover, the parameters need for cavitation started to be studied and some suggested that cavitation could be the primary cause of tissue damage (Fry *et al* 1970, Lele 1977). Cavitation damage was mostly assessed by examining morphological changes after ultrasound exposure. Another important observation was made: when inertial cavitation is induced *in vivo*, mechanical tissue destruction close to blood vessels can result, and the generated bubbles can act as ultrasound scatterers that block wave propagation and subsequent power deposition (Fry *et al* 1970, Lele 1977). On the other hand, studies in simpler fluids revealed that when acoustic cavitation occurs, two physical phenomena are detected: *1.* significant local temperature elevation and *2.* emission of subharmonic or wide band acoustic noise

(Coakley 1971, Eller and Flynn 1969). Lele further demonstrated that transient cavitation *in vivo* produced both subharmonic and ultraharmonic wide band noise emission (Lele 1987). These observations could be used to provide a potentially simple *in vivo* cavitation detection technique.

Focused ultrasound therapy can induce cavitation to mechanically destroy tissue (Fry 1954, Lele 1987). However, the dominant opinion within the ultrasound therapy community has been to avoid cavitation and induce more predictable and controllable thermal damage with focused ultrasound (Fry *et al* 1970, Lele and Pierce 1972, Chapelon *et al* 1996). Despite this prominent reluctance, generated gas bubbles have some potentially useful properties. First, gas bubbles generated from cavitation yield extremely high temperatures and concentrate acoustic energy at the cavitation site. Moreover, theoretical models, extracorporeal, *ex vivo*, *in vitro*, and phantom experimental work have shown that gas bubbles in a focused ultrasound field yield higher ultrasound absorption and therefore higher bulk temperatures in a zone near the focus (Clarke and ter Haar 1997, Holt and Roy 2001, Hynynen 1991, Lele 1987). As a result, higher thermal doses are delivered at the focus; such a gas bubble enhanced heating method could lead to more efficient FUS treatment protocols (Sokka *et al* 2003b). Studies have also shown that the heating effect during thermal mode exposures might be enhanced by occasional cavitation and/or boiling (Bush *et al* 1993, Fry *et al* 1995). Moreover, cavitation activity usually results in atypical lesion sizes and shapes (Sokka *et al* 2003b). To account for a subset of these atypical lesions, thermal models with simple assumptions on bubble distribution and their progression during a sonication have been developed (Chavrier *et al* 2000). In order to explain the enhanced heating effect from a bubble size perspective, bubble kinetics models have also been developed (Holt and Roy 2001). In all of these studies, the induction and timing of cavitation was unpredictable; the overall enhanced heating effect was therefore neither predictable nor controllable (Sokka 2003a).

1.2. *Specific aims*

1.2.1. Theoretical determination and experimental validation of optimal acoustic field for cavitation-based therapy

Of critical importance in ultrasound induced cavitation is to precisely focus the location of cavitation. Ectopic cavitation, that is cavitation outside of the target area, can cause unwanted heating or lesions off focus. In addition, cavitation threshold may vary from point to point in tissue; therefore, locations near the focal point may exhibit cavitation yielding undesired lesions. Ideally, ectopic cavitation could be limited if the cavitation threshold could be preferentially lowered at the transducer focus compared to other areas in field. In this thesis, we tested and optimized dual-frequency methods introduced by Sokka (Sokka 2003a) to preferentially lower the cavitation threshold at the focus relative to the rest of the field. One family of dual-frequency driving waveforms was evaluated in a bubble model incorporating rectified diffusion. Once the optimal waveform shape at the focus was determined, the associated acoustic pressure field was computed from the Rayleigh-Sommerfeld integral. A spherically-curved phased array transducer which yields that waveform at the focus was simulated. The resulting field was further analyzed to determine the relative cavitation threshold in terms of acoustic pressure and intensity. In order to first validate these theoretical predictions in a controlled environment, an *in vitro* experiment was designed and experimental criteria for assessing cavitation activity were used.

1.2.2. *Ex vivo* validation of a dual-frequency method for spatial control of cavitation

As mentioned earlier, our goal was to determine optimal acoustic fields for cavitation-based therapy. We claimed that the combination of a given frequency with its first harmonic would allow surpassing the cavitation threshold at the focus of the transducer while leaving the near field inert. In the *in vitro* validation experiment, we used Optison™, a commercially available contrast agent. However, such a protocol was tightly controlled. As an example, Optison™ has a mean bubble size of 2 - 4.5 μm, which means that the initial bubble radii will fall in this range. Since cavitation threshold has

been proven to depend on this parameter, using ultrasound contrast agents allows for more predictable results. Therefore, in the second part of this thesis, we proposed a focused ultrasound protocol that induces and monitors gas bubbles at the focus and allows for *ex vivo* validation of the theoretical results. The experiments involved fresh rabbit tissue and a statistical analysis was performed over data collected from back muscle. Moreover, the experimental apparatus was designed to be MRI-compatible in order to make future *in vivo* assessments feasible. The study demonstrated that the theoretical predictions made earlier could reliably be used to predict dual-frequency cavitation thresholds. It also suggests that clinical use of dual-frequency excitations might be a solution to the problem of spatial control of cavitation.

2. Theoretical and experimental validation of a dual-frequency excitation method for spatial control of cavitation

2.1. Introduction

Inertial cavitation is a phenomenon which involves bubbles growing to twice their initial size (meaning that their radius grows to twice their initial value) and then having sufficient energy for violently collapse (Duck 1998). Among applications which involve inertial cavitation, focal opening of the blood-brain barrier for drug delivery (Hynynen *et al* 2001) is one of the most promising. Transfection into cells of gene therapy agents also benefits from the presence of microbubbles when sonicated (Greenleaf *et al* 1998). Injected microbubbles (Wu 1998, Miller and Geis 1998, Tran *et al* 2000) or ultrasound-generated bubbles have also been used to enhance heating (Sokka *et al* 2003b) in ablation scenarios. Acoustic cavitation can also activate chemicals and induce tissue damage, which in turn can be enhanced by second-harmonic superimposition (Umemura and Kawabata 1996). In all these techniques, the site of cavitation needs to be precisely controlled in order to tightly localize the therapy. In an application making use of injected microbubbles, such a control is crucial. Since bubbles are present throughout the tissue, off-focal inertial cavitation is even more likely to occur.

In order to either suppress or enhance cavitation at the transducer focus, several researchers have looked into acoustic waveform manipulation methods. Umemura *et al* tackled the problem with a dual-frequency excitation scheme. They summed a fundamental and its associated first harmonic at the focus of two confocal transducers to study the sum's effect on sonodynamic therapy (each transducer was excited by a given frequency). Such a method consists in injecting an anti-tumor agent, which is further cavitated to treat tumors (Umemura and Kawabata 1996). The treatment effect was found to be greatly enhanced by this dual-frequency approach. Chapelon *et al* studied the sonoluminescence activity, the emission of light associated with cavitation, of microbubbles insonified with pseudorandom phase-modulated signals. As a control

experiment, they also sonicated the microbubbles with continuous wave (CW) single frequency ultrasound (Chapelon *et al* 1996). The study demonstrated a significant suppression of the cavitation activity with the proposed method. Bailey *et al* combined a 250-kHz continuous wave with 3-*MHz* pulses at either the positive or negative phase of the lower frequency wave (Bailey *et al* 2002). Their results indicated that superimposing the high frequency pulse on the positive phase yielded higher cavitation activity.

In this thesis, we use a dual-frequency method introduced by Sokka (Sokka 2003a). It allows preferentially lowering the cavitation threshold at the focus relative to the rest of the field for precise control of the cavitation site. Off focal, or ectopic, cavitation activity may thereby be suppressed. The rectified diffusion threshold pressure is used as the cavitation threshold as suggested by earlier works (Umemura and Kawabata 1996).

2.2. *Materials and methods*

2.2.1. The bubble model

In this part, theoretical results are obtained using a code based on Sokka's work (Sokka 2003a). Optimizations and algorithmic variations introduced here will not be discussed as they do not contradict Sokka's predictions.

A two-step method based on Church's work with rectified diffusion was used (Church 1988) in order to calculate the cavitation threshold (the rectified diffusion threshold as discussed earlier) for a given driving waveform. The first step involved the computation of the bubble radius-time curve using the Keller-Miksis bubble model. Once the radius-time curve was determined, it was used as an input to the diffusion equation solutions posed by Eller and Flynn (Eller and Flynn 1965, Keller and Miksis 1980). To complete the second step of the method, the rectified diffusion threshold was derived. The decoupling of these equations was allowed by assuming that rectified diffusion occurs at a slow rate, and especially much slower than bubble oscillations. In other words, Eller and Flynn assumed that negligible diffusion occurs during a single bubble oscillation.

Even if most bubble models are based on the Rayleigh-Plesset equation which models a single bubble in an infinite incompressible medium, the Keller-Miksis equation was selected as it provides a more accurate model. When large range of initial radii and acoustic pressure amplitudes are used as an input to a bubble model, it becomes crucial to include the compressibility of the surrounding fluid. When large enough driving pressures are used in the Rayleigh-Plesset equations, it might result in overestimation of the cavitation threshold and/or convergence problems (Keller and Miksis 1980). On a final note, the more sophisticated Gilmore equation could have provided another refinement as it also includes time-varying thermal effects. However, since its use would have resulted in significant additional computation time, we decided not to use it. Parlitz *et al* provided a formulation of the Keller-Miksis equation (Parlitz *et al* 1990):

$$\left(1-\frac{\dot{R}}{c}\right)R\ddot{R}+\frac{3}{2}\dot{R}^2\left(1-\frac{\dot{R}}{3c}\right)=\left(1-\frac{\dot{R}}{c}\right)\frac{P(\dot{R},R,t)}{\rho}+\frac{R}{\rho c}\frac{\partial P(\dot{R},R,t)}{\partial t} \quad (1)$$

with

$$P(\dot{R},R,t)=\left[\left(p_0-p_v+\frac{2\sigma}{R_0}\right)\left(\frac{R_0}{R}\right)^{3\kappa}+p_v\right]-p_0-\frac{2\sigma}{R_0}-\frac{4\mu\dot{R}}{R}-P_a \quad (2)$$

Table 2-1 summarizes the values of constants that were used (Lauterborn 1976).

Constant	Description	Value
p_o	Hydrostatic Pressure	100 kPa
p_v	Vapor Pressure	2330 Pa
c	Sound Speed	1500 m/s
Σ	Surface Tension	0.0725 N/m
M	Shear Viscosity of Liquid	0.001 N·s/m^2
ρ	Liquid Density	998 kg/m^3
K	Polytropic Exponent	1.33

Table 2-1. Constants used in the Keller-Miksis bubble model

To come up with this equation, experiments involving a single bubble in an acoustic field were conducted. As a result, the Keller-Miksis equation models the wall motion *R(t)*, of this bubble characterized by an initial radius R_0, when stimulated by an acoustic driving pressure, *Pa(t)*.

A couple of assumptions are incorporated in the model (Edson 2001). First of all, the bubble is assumed to be surrounded by water, which is infinite in extent. The water is also assumed to behave as a compressible liquid, which represents an improvement over the Rayleigh-Plesset equation, and to be a Newtonian fluid (surface tension is included in the analysis). Before any acoustic field is applied, there is a single bubble in the water, which is characterized by its initial radius, R_o. This bubble exists in water at $t=0^-$, and is filled with a gas, which is assumed to obey the polytropic gas law. Moreover, both

temperature and pressure have uniform spatial distribution within the bubble. When insonified, this bubble may only undergo spherical oscillations and/or collapse, and mass and heat transfer between the bubble and the liquid are neglected. Shear viscosity and viscous dissipative effects are both included. On a final note, the forcing pressure field is time-dependent, and the external ambient (or hydrostatic) pressure is assumed to be constant.

It is important to notice that these assumptions are only accurate in a situation where a single bubble cavitates in water. As described and discussed later in this thesis, experiments did not involve a single bubble in an acoustic field, but rather a cloud of bubbles, either injected (contrast agent microbubbles), or naturally present in tissue. When cavitation occurs in biological tissue, the model described above may not account for every single additional complexity inherent to the medium. First of all, tissue is generally assumed to be non-Newtonian because of its viscoelastic properties. Besides, cavitation *in vivo* is not necessarily initiated from a single bubble in a fluid which is infinite in extent, as assumed in the Keller-Miksis model. In biological tissue, a more common situation would consist in having multiple bubbles in compartmentalized tissues. Even if experimental situations seem rather complicated as compared to assumptions associated with the Keller-Miksis model, there are still ways to better fit the model to real situations. We can first assume that i*n vivo* cavitation is initiated from seed bubbles. A value of $R_0 = 1\ \mu m$ may be used to reflect the initial seed bubble radii in tissue (Church 1988). Besides, these bubbles are generally located in areas that allow them some room to oscillate whether it is in the interstitial space or blood vessels. Such a variability in surrounding conditions will affect the bubble behavior but is beyond the scope of this thesis.

In summary, differences between real experimental conditions and model's assumptions may prevent us from predicting absolute cavitation threshold values in tissue. However, it may still be used to compare the impact of different waveforms on bubble dynamics and to estimate relative cavitation thresholds.

Another limitation of the Keller-Miksis bubble model is that mass transfer is not accounted for. However, in the second step of the method, the calculation of cavitation

thresholds itself makes use of the Eller and Flynn rectified diffusion equation, which incorporates it.

In order to determine the rectified diffusion threshold, which will further be used as the cavitation threshold, the gas flux into the bubble was calculated over multiple acoustic cycles given a periodic solution to the bubble dynamics equation (Eller and Flynn 1965). The time rate of change of the moles of gas n in the bubble is formulated below:

$$\frac{dn}{dt} = 4\pi R_0 D\left[A + R_0\left(\frac{B}{\pi Dt}\right)^{1/2}\right]C_{sn}\left(\frac{C_i}{C_{sn}} - \frac{A}{B}\right) \tag{3}$$

$$\text{With } A = \frac{1}{T_b}\int_0^{T_b}\frac{R}{R_0}dt, \tag{4}$$

$$\text{and } B = \frac{1}{T_b}\int_0^{T_b}\left(\frac{R}{R_0}\right)^4 dt, \tag{5}$$

$$\text{and } C_{sn} = C_0\left[1 + \frac{2\sigma}{R_0 P_0}\right] \tag{6}$$

As in all equations listed in this thesis, R_0 is the equilibrium or initial radius of the bubble, D is the diffusion constant, C_i is the concentration of dissolved gas in the liquid, and C_0 is the saturation concentration of gas in the liquid. In order to represent an air filled bubble, a gas saturation percentage value of $C_i/C_0 = 0.857$ was used (Church 1988). A and B were calculated from the solution to the Keller-Miksis equation given a forcing waveform, $P(t)$. In both A and B expressions, T_b is the period of bubble wall motion $R(t)$ in steady state. The period of the bubble wall motion is generally equal to a multiple of

the period of the forcing function (or forcing waveform). In the case of a dual-frequency waveform, this period is equal to the period associated with the highest frequency (the first harmonic). A and B were computed for different multiples of this period, 1 to 5, in successive time regions in steady state of the radius-time curve. The recursive computation of A and B over the adjacent time regions was terminated as soon as the calculated values were within 0.1 %. Those values of A and B were then used in the calculation of the rectified diffusion threshold. By definition, the rectified diffusion threshold is the minimum pressure at which there is a net flux of gas into the bubble. In terms of calculations, this implies to determine the zero of Equation 3 (this was done for different amplitudes of the forcing pressure waveform). The zero of Equation 3 corresponds to $A/B = C_i/C_{sn}$; therefore, the minimum pressure amplitude at which this occurred was noted as the cavitation threshold.

The block diagram presented in Figure 2-1 summarizes all the necessary steps in order to determine cavitation thresholds.

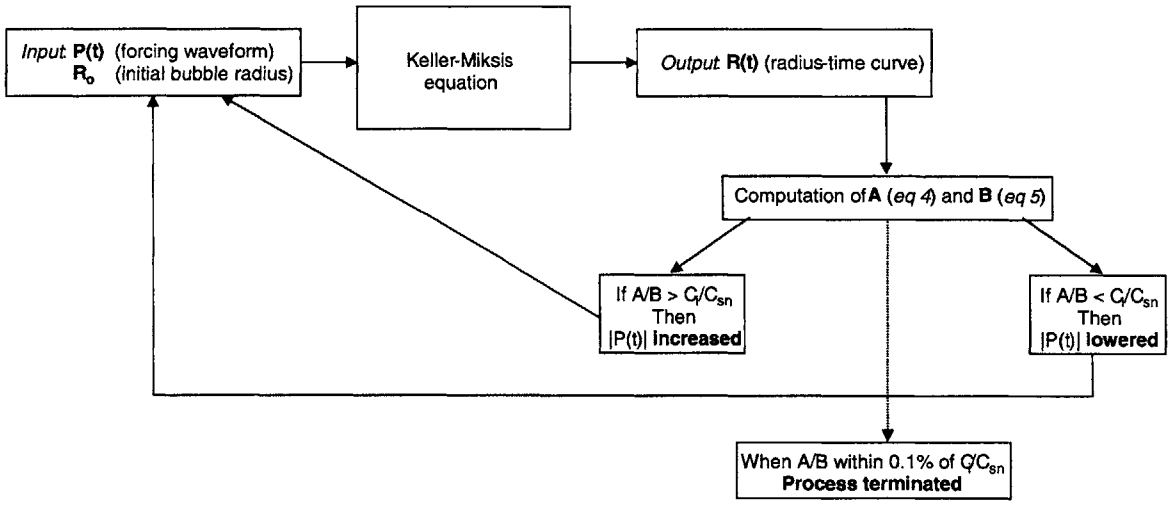

Figure 2-1. Block diagram representing all the necessary steps in order to determine cavitation thresholds

In summary, the computation of the cavitation threshold associated with a given waveform required several steps. The radius-time curve $R(t)$ was first calculated making use of the Keller-Miksis equation. At that point, an initial test pressure amplitude was used as the input to this equation. In a second step, A and B were computed and further compared to C_i/C_{sn}. The value of A/B was then discussed; if it was greater than C_i/C_{sn}, the pressure amplitude was raised (above the initial test pressure amplitude value). Otherwise if A/B was less than C_i/C_{sn}, the pressure amplitude was then lowered (below the initial test pressure amplitude value). The process was terminated when A/B was found to be within 0.1 % of C_i/C_{sn}. The pressure amplitude used to achieve such a result represented the cavitation threshold associated with the tested waveform.

2.2.2. Tested dual-frequency waveforms

The cavitation thresholds for a family of driving waveforms were calculated. The set of waveforms consisted of the sum of two equal amplitude but different frequency cosines, $P_{ac}\left(0.5\cos(2\pi ft)+0.5\cos(2\pi 2ft+\theta)\right)$, where θ was varied from 0 to 2π. Figure 2-2 shows the waveform shapes for a subset of this family for five different values of θ.

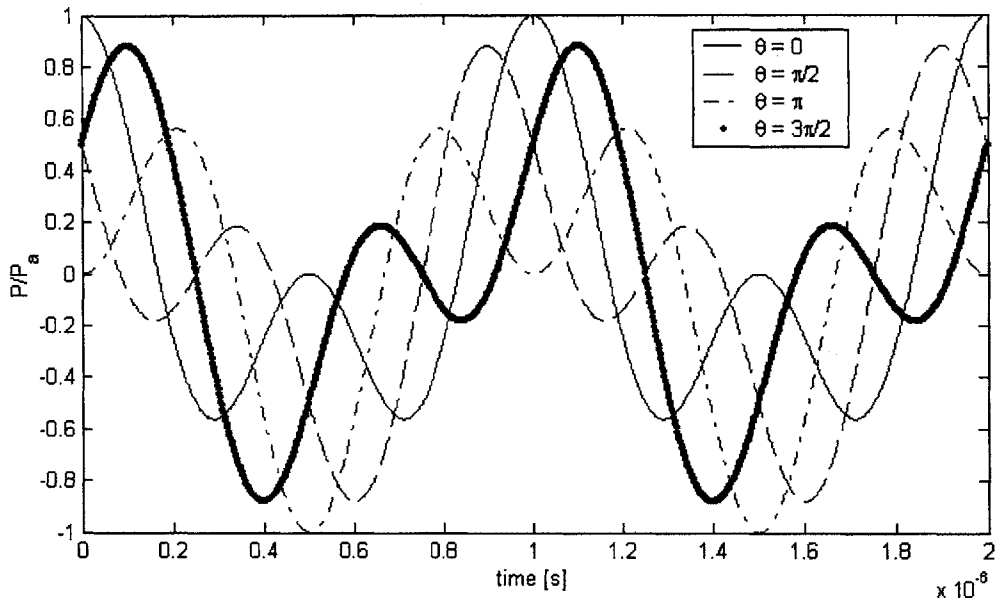

Figure 2-2. Family of curves calculated from $P_{ac}\left(0.5\cos(2\pi ft)+0.5\cos(2\pi 2ft+\theta)\right)$, where θ is varied from *0* to 2π

2.2.3. Experimental verification of theoretical results

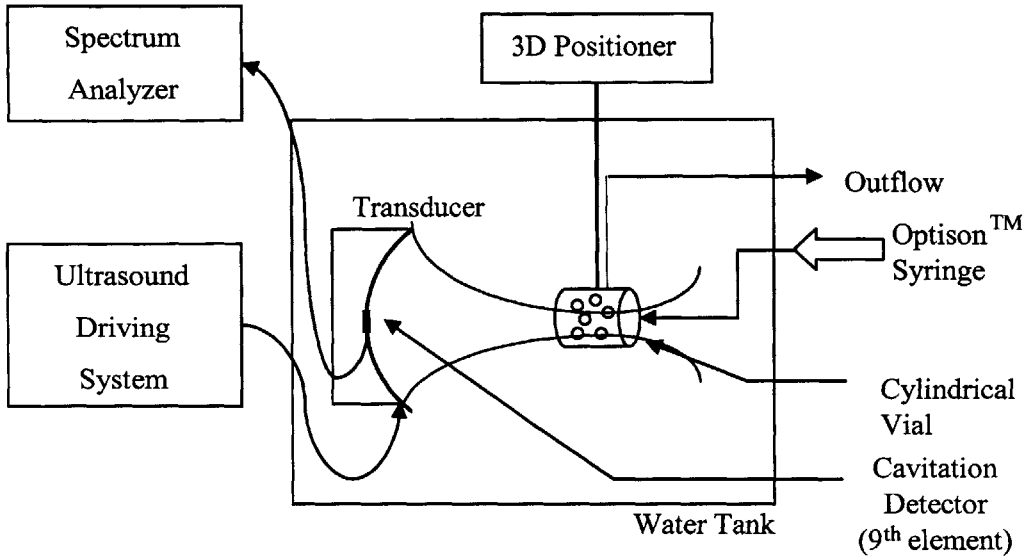

Figure 2-3. Experimental setup for measuring cavitation threshold for dual-frequency waveforms

The threshold variation observed in simulation was verified experimentally. Figure 2-3 shows the experimental setup (designed by Gauthier and Sokka) for measuring cavitation threshold for different dual frequency waveforms. An eight-sector, focused, piezocomposite transducer array (10 cm diameter, 8 cm radius of curvature, manufactured by Imasonic, France), driven by a multi-channel broadband ultrasound driving system designed in house (Sokka *et al* 2003c), was used to generate the dual-frequency field in a water tank. A 2.5 *cm* diameter by 2.5 *cm* long cylindrical vial was filled with a mixture of degassed water and Optison™ (Mallinckrodt Medical, St. Louis, MO), a commercial microbubble contrast agent. The focus of the transducer was positioned to be in the center of this vial. The plastic cylindrical vial was capped on both ends with Mylar membranes to allow the passage of the ultrasound beam through the chamber. A concentration of 0.015 ml of Optison™ per ml of water was maintained in the vial. In order to ensure that no large air bubbles were trapped in the chamber, the microbubble mixture was circulated into the vial until liquid was observed on the outflow

line. Prior to sonication, the cylindrical vial was slightly agitated to keep microbubbles in suspension. During insonation, the transducer's center circular element (diameter = 2 cm) was connected to a spectrum analyzer (Hewlett-Packard 8590A) and used as a passive cavitation detector. Similar to earlier *in vivo* experiments (Lele 1977, Hynynen 1991), the presence of broadband subharmonic emission was used to assess inertial cavitation.

Below are two figures, which are representative of: *1.* the acoustic signal coming back from the vial wherein Optison™ microbubbles are not cavitating (Figure 2-4(a)) and *2.* the acoustic signal coming back from the vial wherein Optison™ microbubbles are cavitating (Figure 2-4(b)).

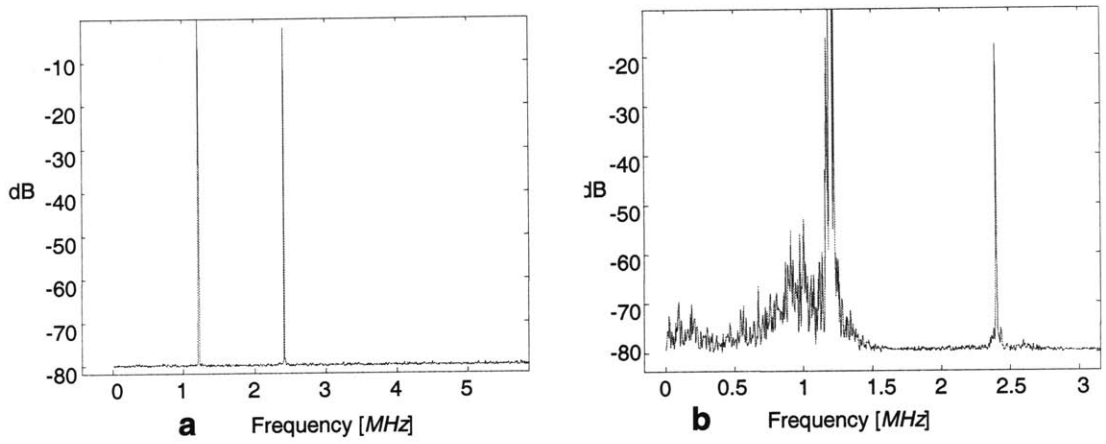

Figure 2-4. (a) Magnitude of the FFT of an acoustic signal without cavitating Optison™ microbubbles. The absence of broadband subharmonic emission indicates that there is no inertial cavitation activity. **(b)** Magnitude of the FFT of an acoustic signal in the presence of cavitating Optison™ microbubbles. The presence of broadband subharmonic emission indicates inertial cavitation activity

Here is the methodology that we followed when measuring the cavitation threshold at the geometrical focus of the transducer. The situation where the vial was moved along the transducer axis in order to measure the cavitation threshold at different locations along the transducer axis is discussed in the upcoming section. For each tested waveform, that is, for each tested value of θ, the input voltage was raised until inertial cavitation was observed at the geometrical focus of the transducer. Since the driving voltage is linearly proportional to the driving pressure, the voltage level at which inertial

cavitation occurred was recorded as the corresponding cavitation threshold. On a final note, Optison™ has a mean bubble diameter of 2-4.5 μm, so the results from experiment were compared with simulation results with $2R_0$ in this range.

The phase control capabilities of the multi-channel broadband ultrasound driving system designed in house were assessed by recording the pressure at the focus using a 0.075 mm needle hydrophone. Several first harmonic phase values were tested in order to make sure that the ultrasound driving system could reliably generate dual-frequency fields. Below are two figures representing hydrophone recordings for two different first harmonic phase values: 0° (Figure 2-5(a)), and 180° (Figure 2-5(b)).

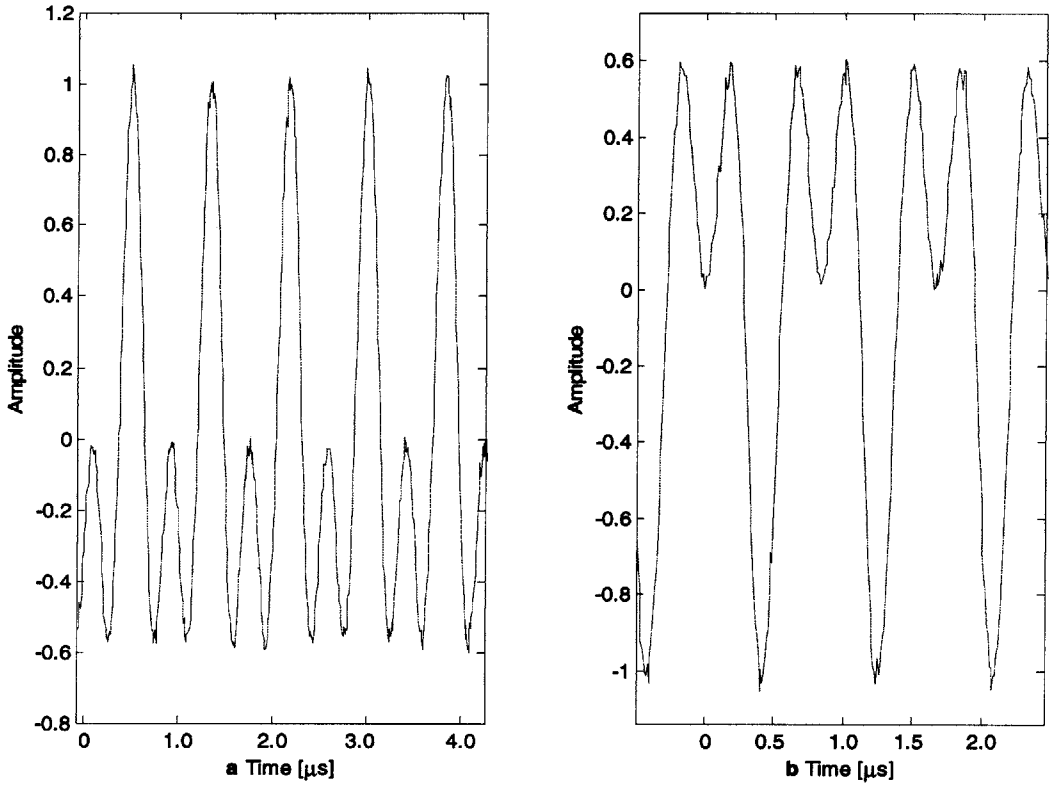

Figure 2-5. Hydrophone recordings at the geometrical focus of the transducer for two different first harmonic phase values. **(a)** 0° **(b)** 180°

2.2.4. Acoustic field and cavitation field calculations

In a former study, Sokka introduced the concept of cavitation field (Sokka 2003a). He defined the cavitation field as the relative cavitation threshold in space for a given acoustic field. Given the acoustic field, the pressure waveform at each point in space is known. This pressure waveform can then be used as an input in order to compute the cavitation threshold using the model described earlier. When the acoustic field is a single-frequency field, one may expect that all points in space will be stimulated by similar waveforms varying only by phase. Therefore the cavitation field is expected to be constant, providing that the CW (Continuous Wave) mode is used. If now the field is multi-frequency in nature, different waveforms will stimulate different points in space. As a result, different cavitation thresholds will result in space as well. Two parameters come therefore into play to shape the cavitation field: *1.* the transducer geometry and *2.* the specific excitation of the transducer (the driving signal to each element of the transducer). For this study, we computed the cavitation field for an 8-sector array with dual-frequency excitations. For all dual-frequency fields, alternating elements were driven at the two different frequencies. The Rayleigh-Sommerfeld integral (Zemanek 1971) was used to calculate the acoustic field for the transducer. The pressure field from an ultrasound element through a lossy substrate can be modeled as:

$$p(\mathbf{r}) = \frac{i\rho_o ck}{2\pi}\int_A \frac{e^{-ik(\mathbf{r}-\mathbf{r}')}e^{-\mu d}u}{\mathbf{r}-\mathbf{r}'}dA \qquad (7)$$

where ρ_o is the tissue density, c is the speed of sound, k is the wave number ($2\pi/\lambda$), λ is the ultrasonic wavelength, $\mathbf{r}$ is the coordinate vector (x,y,z) of the pressure point, $\mathbf{r}'$ is the coordinate vector of the incremental source area of the complete transducer area A, μ is the attenuation coefficient in the lossy material (absorption and scattering), d is the ray distance in the lossy material between the source point and the location of the desired pressure point, and $\mathbf{u}$ is the complex surface velocity of that source (magnitude and phase). If now one considers an array made of N elements, the pressure at a given point m corresponding to a location (x_m, y_m, z_m) is given by:

$$p_m = \sum_{n=1}^{N} \frac{i\rho ck}{2\pi} \int_A \frac{e^{-ikr_{mn}} e^{-\mu d} u_n}{r_{mn}} dA \qquad (8)$$

where subscript n corresponds to the driving signal of the nth element of the array. In this model, temperature, non-linear, refraction, and scattering effects on pressure calculation are neglected. Besides, the attenuation term is also neglected for our purposes. The aforementioned integral computes the complex pressure for a single frequency field. Therefore, two separate arrays were used to model the 8-sector array for dual-frequency excitations. The resulting fields were then summed in the time domain using $P_1 \cos(2\pi f_1 t + \theta_1) + P_2 \cos(2\pi f_2 t + \theta_2)$, where P_1 and θ_1 are the magnitude and angle of the complex pressure at f_1 and P_2 and θ_2 are magnitude and angle of the complex pressure at f_2. Given the time-varying field in space, the cavitation threshold at various points may then be computed using the model described earlier.

2.2.5. Experimental determination of cavitation field

The same experimental setup as described before can be used here to confirm the simulation results. In previous experiments, the focus of the transducer was positioned to be in the center of the cylindrical vial and then the only varying parameter was the phase between the fundamental and the first harmonic frequency components. Here the situation was slightly different. Since we wanted to determine the cavitation threshold along the transducer axis, we had to move the vial along its axis while keeping the transducer still. For each given position of the vial, the input voltage was raised until inertial cavitation was observed. The acoustic pressure corresponding to the input voltage for which inertial cavitation was observed was then recorded by replacing the vial by a hydrophone. For each given location, the cavitation threshold was finally calculated by dividing the recorded input voltage by the corresponding acoustic pressure, which was the recorded hydrophone voltage.

As a control experiment, we sonicated the vial with only one of the two aforementioned frequencies. That is all the 8 sectors were sending in phase a 2.4-*MHz* CW (Continuous Wave) pulse.

2.3. Results

2.3.1. Relative cavitation thresholds for various families of pressure waveforms

The relative cavitation thresholds obtained with the set of tested waveforms is shown in Figure 2-6. Each curve corresponds to a different fundamental frequency. Fundamental frequencies equal to 1.2, 2.4, 3.0, and 3.6 *MHz* were tested. For lower fundamental frequencies, 1.2 and 2.4 *MHz*, the waveforms showed a differential in the cavitation threshold with a first harmonic phase in the 180-220° range showing the lowest threshold. This waveform family may be useful to create a differential cavitation field as the equal amplitude sinusoids combined at various phases in the field will create a widely varying acoustic field.

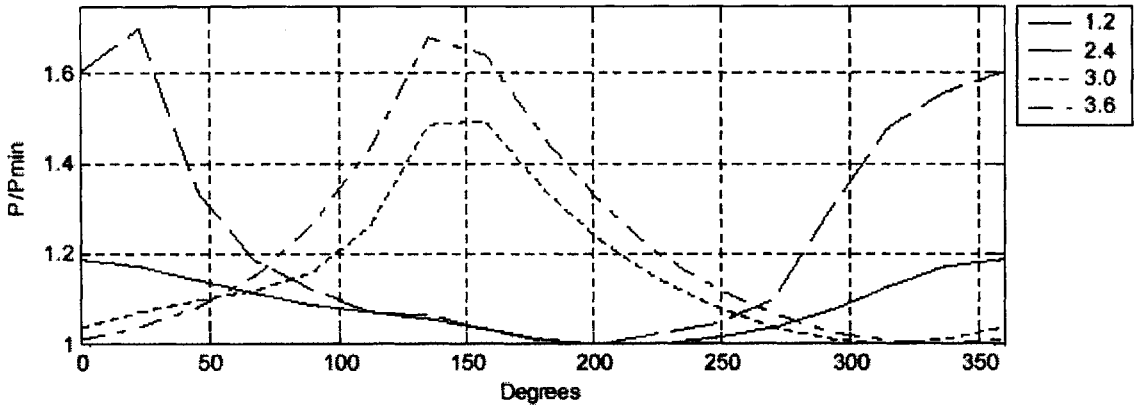

Figure 2-6. Relative cavitation threshold for the tested family of curves where equal amplitude sinusoids of the fundamental and first harmonic are combined with the first harmonic having a variable phase delay

2.3.2. Experimental validation of relative cavitation thresholds

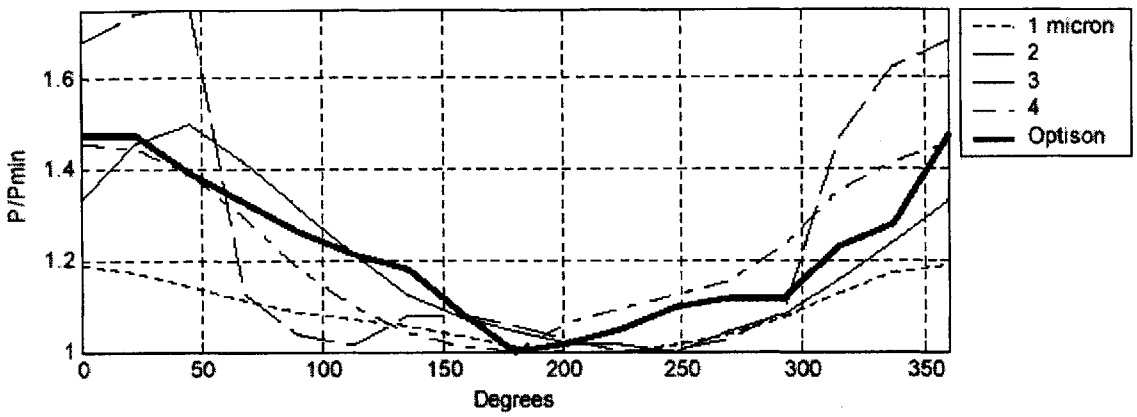

Figure 2-7. Relative cavitation thresholds for dual-frequency equal amplitude excitation where the phase of the second harmonic is varied for various values of R_0 with the data from experiments with Optison™ overlaid

To verify the reliability of Sokka's cavitation threshold model, the results from experiments with Optison™ were compared with predictions from the simulations. For the *in vitro* experiments, the Optison™ sample was insonified with the focal pressure profile generated from the tested waveform family, that is the combination of equal amplitude sinusoids with the phase delay of the first harmonic varied. Figure 2-7 shows the results of both the *in vitro* experiment and simulations from bubble diameters of 1 to 4 μm. As noted earlier, such a diameter range is representative since the mean diameter of the Optison™ microbubbles is between 2 and 4.5 μm. The experimental data follows the model results from the 3 and 4 μm bubble very closely. The trends were consistent and the minimum and maximum relative cavitation thresholds were almost identical. The predictions from the model correlated very well with the results from the controlled *in vitro* experiment.

2.3.3. Cavitation fields generated from dual-frequency acoustic fields

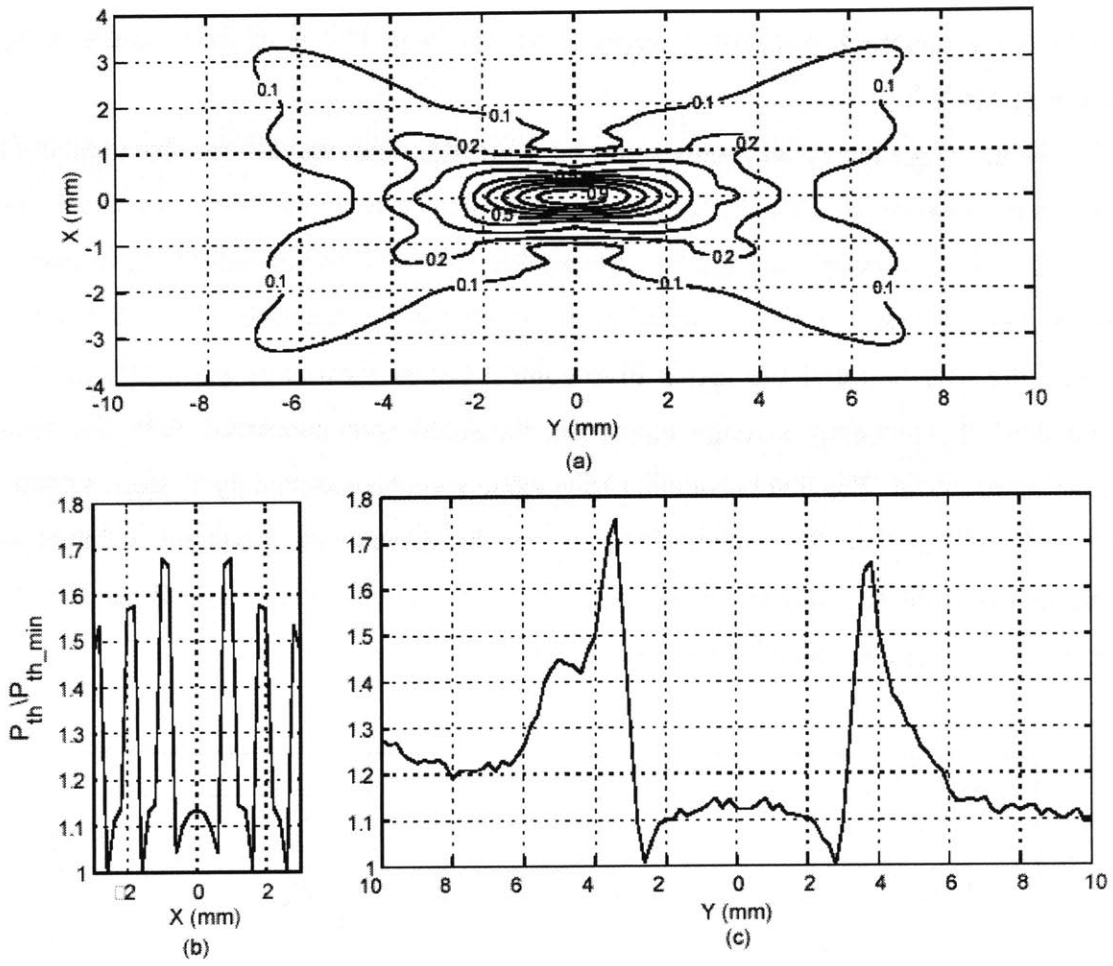

Figure 2-8. Acoustic and cavitation fields of a dual-frequency equal amplitude ultrasound exposure aimed at generating a lower cavitation threshold at the focus using a waveform from the tested waveform family

(a) The acoustic field near the focus oriented with the transducer to the left

(b) The cavitation field along the x-axis in the focal plane

(c) The cavitation field along the transducer axis

The graphs shown in Figure 2-8 are the field patterns resulting from combining two equal amplitude sinusoids with the first harmonic signal having a phase of 210^{o} at the focus. This phase angle exhibited the lowest cavitation threshold among the tested waveforms. The focal size as measured from Figure 2-8(a) is 0.9 mm x 4.4 mm. Figure 2-8(b) shows larger threshold maxima surrounding the focus with a maximum threshold

value 50 % larger than at the focus. Figure 2-8(c) shows similarly high maxima along the axis of the transducer. In addition, a higher threshold in the nearfield than at the focus was observed for the entire nearfield region shown in the plot and continues beyond. To cavitate in the nearfield, pressures ranging from 110 % to 150 % of the pressure at the focus were needed.

To see if greater differentials could be achieved, other waveforms from the same family were evaluated. This time, we tried specifically to lower the focal cavitation threshold relative to nearfield cavitation thresholds. To do so, we evaluated the impact of different first harmonic phases and tried to maximize the cavitation threshold differential between the nearfield and the focus. Five control points located in the nearfield were chosen and the resulting average cavitation threshold was compared with the focal cavitation threshold. The first harmonic phase value was incremented by 5° steps between 150° and 250°. Figure 2-9 summarizes the results. Cavitation threshold differentials obtained for different values of the first harmonic phase were normalized by the maximum cavitation threshold differential value that we found.

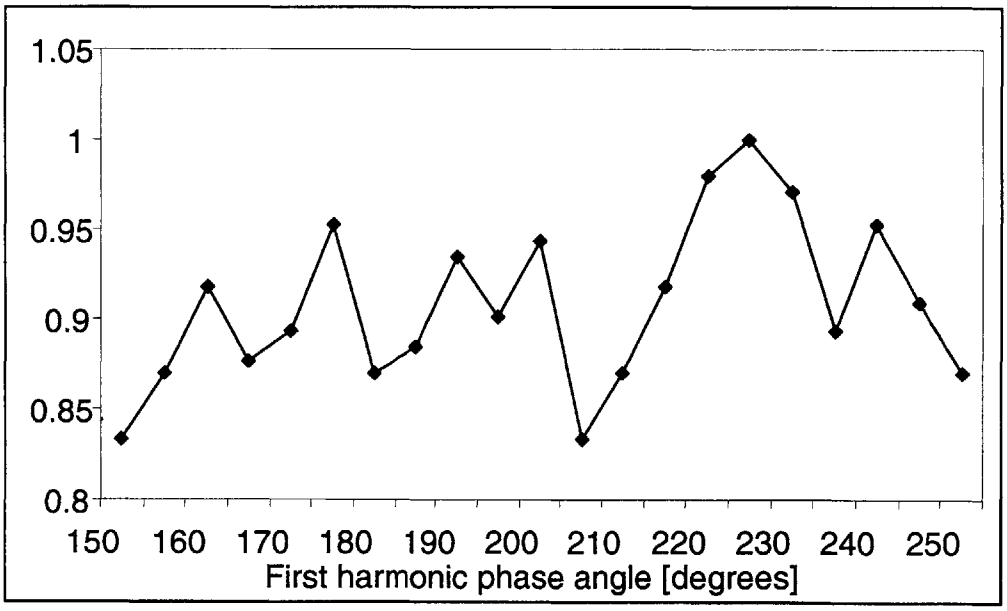

Figure 2-9. Nearfield to focal point cavitation threshold differential. The first harmonic phase value was varied from 150° to 250°

Among the best nearfield to focal point threshold differentials resulted from the pattern with first harmonic phase angle of 225°. The focus from this field has similar dimensions to the one exhibited in Figure 2-8. Moreover, the x-axis cavitation field was also not remarkably different. However, the cavitation field along the transducer axis presented in Figure 2-10 shows significant improvement over the previous field.

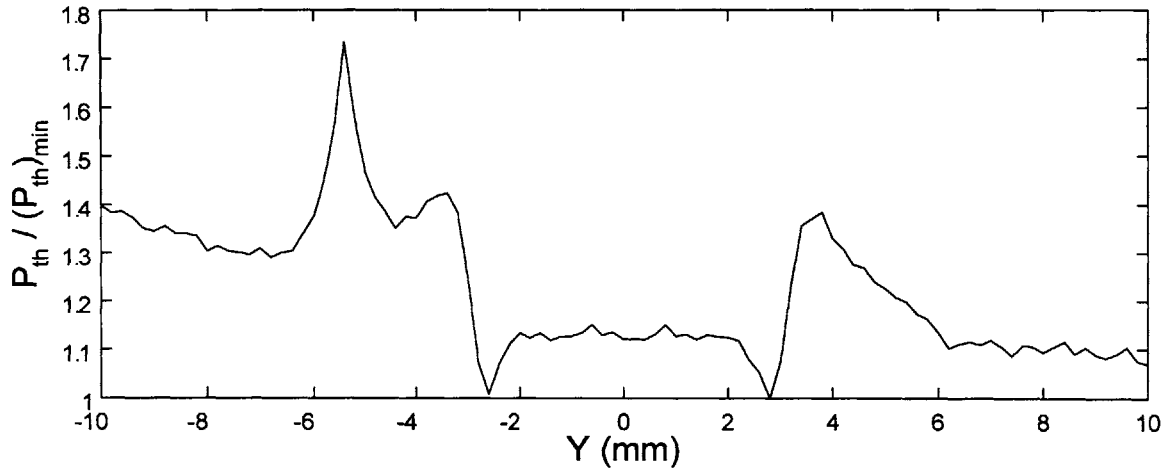

Figure 2-10. Cavitation field along the transducer axis from equal amplitude dual-frequency exposure optimized to generate a large nearfield to focal point threshold differential

The cavitation threshold in the nearfield ranges from 117 % to 153 % of the threshold at the focus with a space-averaged threshold of nearly 122 % of the threshold at the focus. This differential is a significant improvement over a single-frequency field, which exhibits a uniform cavitation field.

In summary, when a bubble is sonicated with a dual-frequency field characterized by a first harmonic phase angle of 225°, initiating cavitation in the nearfield requires 48 % higher intensities (intensity and power vary as pressure squared) than that found at the focus.

As mentioned earlier, the model used here to determine relative cavitation thresholds assumed a homogeneous medium (Sokka 2003a). Even if tissue is not homogeneous, significant tissue factors that lower the threshold in the nearfield would be needed to overcome this higher threshold barrier.

2.3.4. Experimental validation of cavitation fields

Again, the reliability of Sokka's cavitation model was assessed by running an experiment with Optison™ and comparing the results with predictions from simulations. As described in the Materials and Methods section, the dual-frequency cavitation field generated with a first harmonic phase angle of 225° was measured and is displayed in Figure 2-11. The experimental cavitation threshold in the nearfield ranges from 116 % to 135 % of the threshold at the focus. These results show a significant improvement over a single-frequency sonication, which led to a relatively uniform cavitation threshold field, as displayed in Figure 2-12. In both sets of experiments, presented in Figure 2-11 and Figure 2-12, measurements were repeated 5 times; the displayed curves represent average measurement results.

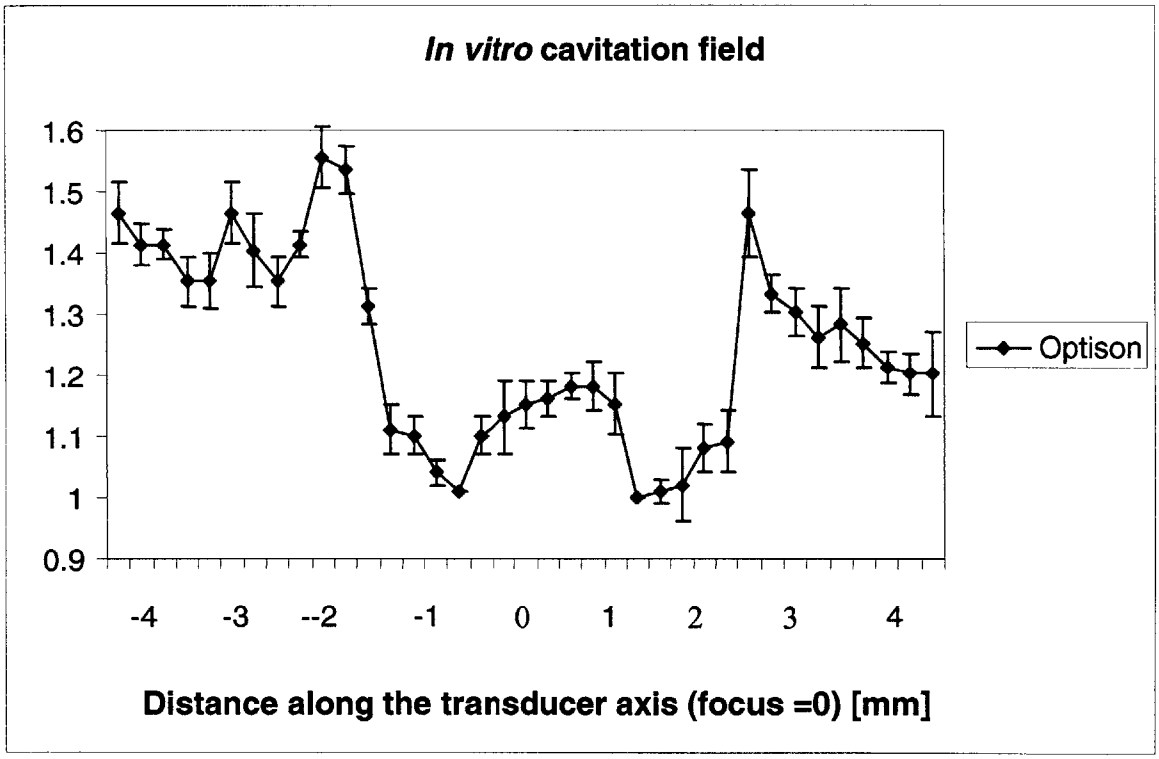

Figure 2-11. Experimental cavitation field along the transducer. First harmonic phase angle is equal to 225°.

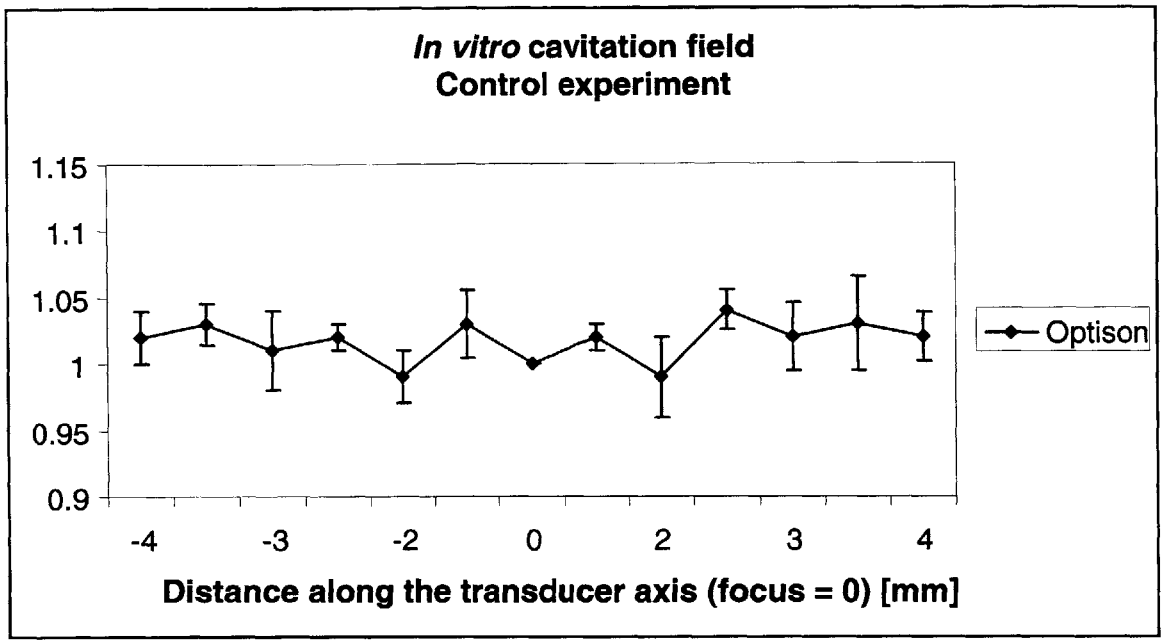

Figure 2-12. Experimental cavitation field along the transducer. Control experiment (the 8 sectors were sending in phase a 2.4-*MHz* CW (Continuous Wave))

3. Spatial control of cavitation: *ex vivo* validation of a dual-frequency method

3.1. Motivation

As emphasized in the first part of this thesis, the combination of a given frequency with its first harmonic would allow surpassing the cavitation threshold at the focus of the transducer while leaving the near field inert. In the first part of this thesis, we used Optison™, a commercially available contrast agent, to design an *in vitro* experiment, which confirmed the theoretical predictions initially made by Sokka (Sokka 2003a) and refined here. However, such a protocol is tightly controlled. As an example, Optison™ has a mean bubble diameter of 2-4.5 μm, which means that the initial bubble diameters will fall in this range. Since cavitation threshold has been proven to depend on this parameter, using ultrasound contrast agents allows for more predictable results. In the second part of this thesis, we propose a focused ultrasound protocol that induces and monitors gas bubbles at the focus and allows for *ex vivo* validation of the aforementioned theoretical results. The experiments involved fresh rabbit tissue and a statistical analysis was performed over data collected from back muscle. Moreover, the experimental apparatus was designed to be MRI-compatible to make future *in vivo* assessments feasible. The study demonstrates that the experimental results can reliably be used to predict dual-frequency cavitation thresholds. It also suggests that clinical use of dual-frequency excitations might be a solution to the problem of spatial control of cavitation.

3.2. Materials and methods

3.2.1. Focused ultrasound therapy transducer

The same eight-sector transducer as described in Chapter *2* of this thesis was used in the experiments. In all experiments, half of the sectors were driven with an identical radio frequency (RF) signal while the other half was driven with another RF signal. The first RF signal had a frequency of 1.2 *MHz* and was generated by a Hewlett Packard 33120A arbitrary waveform generator and amplified by an ENI 2100L RF power amplifier, which could provide a 50dB gain in the frequency range 10 kHz-12 *MHz*. The other RF signal had a frequency of 2.4 *MHz* and was generated by an Agilent 33250A arbitrary waveform generator and amplified by another similar ENI 2100L RF power amplifier. A total electrical power of 400 W was available. A preliminary experiment consisted in driving only half of the sectors, either the 1.2 *MHz*- or 2.4 *MHz*-driven ones, so as to measure the resulting acoustic pressure at the geometrical focus of the transducer. A 0.075 mm needle hydrophone recorded the pressure at the focus, which is proportional to the hydrophone voltage, and allowed for calibration of the driving signals. The amplitude of the two driving electrical signals was adjusted so that the resulting focal pressure amplitudes were equal. As in Chapter *2* of this thesis, we also checked the phase control capabilities of the waveform generators. Below are two figures representing hydrophone recordings for two different sets of input waveforms. In the first set, the 8 sectors of the transducer were sending in phase a 1.2-*MHz* 5-μs burst (Figure 3-1(a)). In the second set, alternating sectors were sending 1.2-*MHz* and 2.4-*MHz* 5-μs bursts, the first harmonic phase value being set to 180^0 (Figure 3-1(b)).

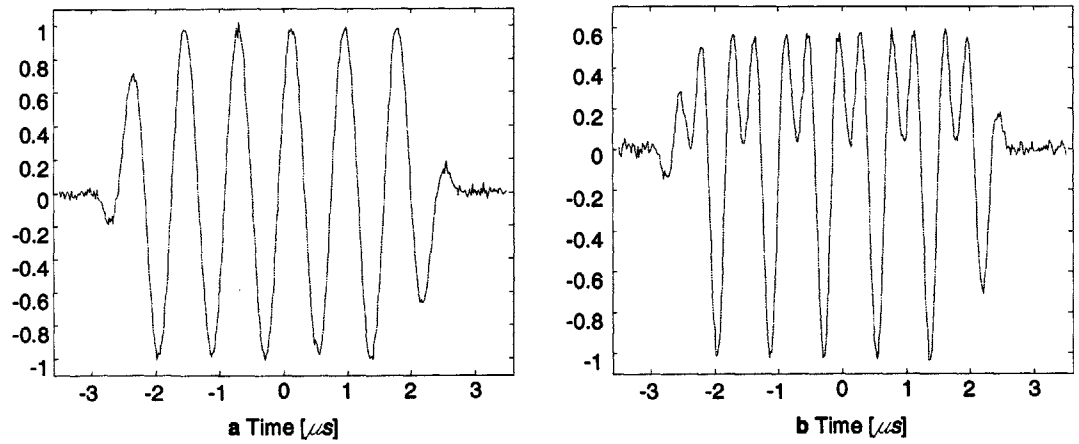

Figure 3-1. Hydrophone recordings at the geometrical focus of the transducer for two different sets of input waveforms. **(a)** the 8 sectors of the transducer were sending in phase a 1.2-*MHz* 5-μs burst **(b)** alternating sectors were sending 1.2-*MHz* and 2.4-*MHz* 5-μs bursts, the first harmonic phase value being set to 180°

3.2.2. Sonications

In this experiment, the same set of waveforms as previously used in the first part of this thesis was evaluated. They were the sum of two equal amplitude but different frequency cosines. Figure 2-2 shows the waveform shapes for a subset of this family for five different values of Θ. Since the phase between the two waveforms had to be precisely adjusted, both arbitrary waveform generators were used in triggered burst phase-lock mode. In the triggered burst mode, phase-lock signals can be synchronized using an external trigger. A second Hewlett Packard 33120A arbitrary waveform generator was used as an external trigger and synchronized the two arbitrary waveform generators.

Single burst duration, 5 μs, was tested. Below are graphical representations of the two bursts (one at 1.2 *MHz*, Figure 3-2(a); the other at 2.4 *MHz*, Figure 3-2(b)). Both bursts were acquired with a Yokogawa 7100 storage oscilloscope at a sampling frequency of 50 *MHz*.

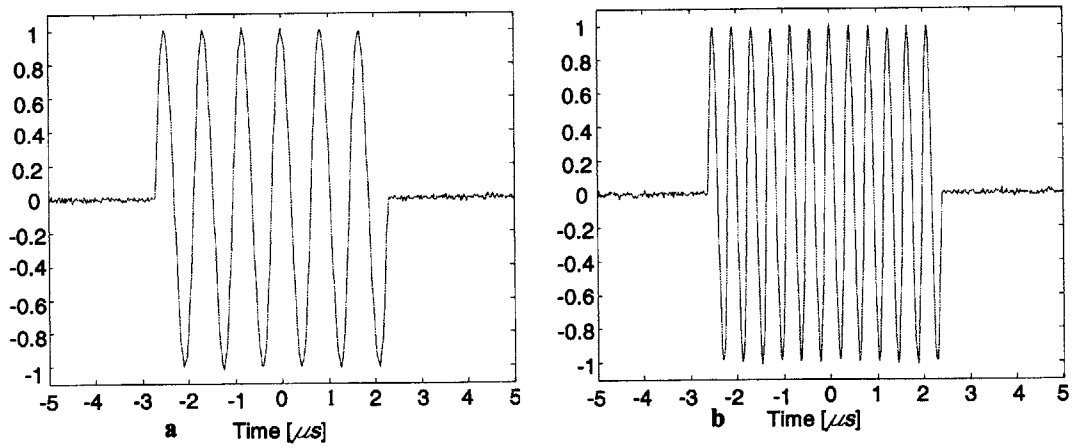

Figure 3-2. (a) 1.2 *MHz* 5-μs burst captured by a Yokogawa 7100 storage oscilloscope. **(b)** 2.4 *MHz* 5-μs burst captured by a Yokogawa 7100 storage oscilloscope

In order to measure the cavitation threshold at the focus, the same methodology as described in Chapter *2* of this thesis was used. The input voltage was raised until cavitation was observed. The driving voltage being linearly proportional to the driving pressure, the voltage level at which cavitation is observed is proportional to the threshold pressure. As a control, the same protocol was repeated with Optison™, a commercially available contrast agent, whose response to dual-frequency sonications has already been studied (Sokka 2003a).

3.2.3. Cavitation detector

In order to detect gas bubble activity, the transducer's center circular element, the 9th element, was used. The detected signal was buffered and filtered by a LeCroy DA1820A differential amplifier (Chestnut Ridge, NY) with 10 $M\Omega$ input impedance and a band pass filter range of 10 *kHz* - 3 *MHz*. The signal was then captured over a 50 μs window by a Yokogawa 7100 storage oscilloscope (Tokyo, Japan) at a sampling rate of 50 *MHz*. The captured signals were transferred to a computer and their Fast Fourier Transforms were computed. The resulting spectrums were then inspected for subharmonic acoustic emission, which is a characteristic of bubble oscillation (Lele 1977,

Hynynen 1991). A broadband noise in the subharmonic region denoted bubble collapse, also known as inertial cavitation.

3.2.4. Experimental protocol

After unrelated experiments, New Zealand white rabbits (male, approximately 4 *kg*) were sacrificed as a part of that study. Back muscle was then harvested and samples were used right after. They were approximately 1.5 *cm* thick, 3 by 3 *cm* samples of back muscle.

3.2.4.1. *Ex vivo* experiment: determination of relative cavitation threshold versus first harmonic phase

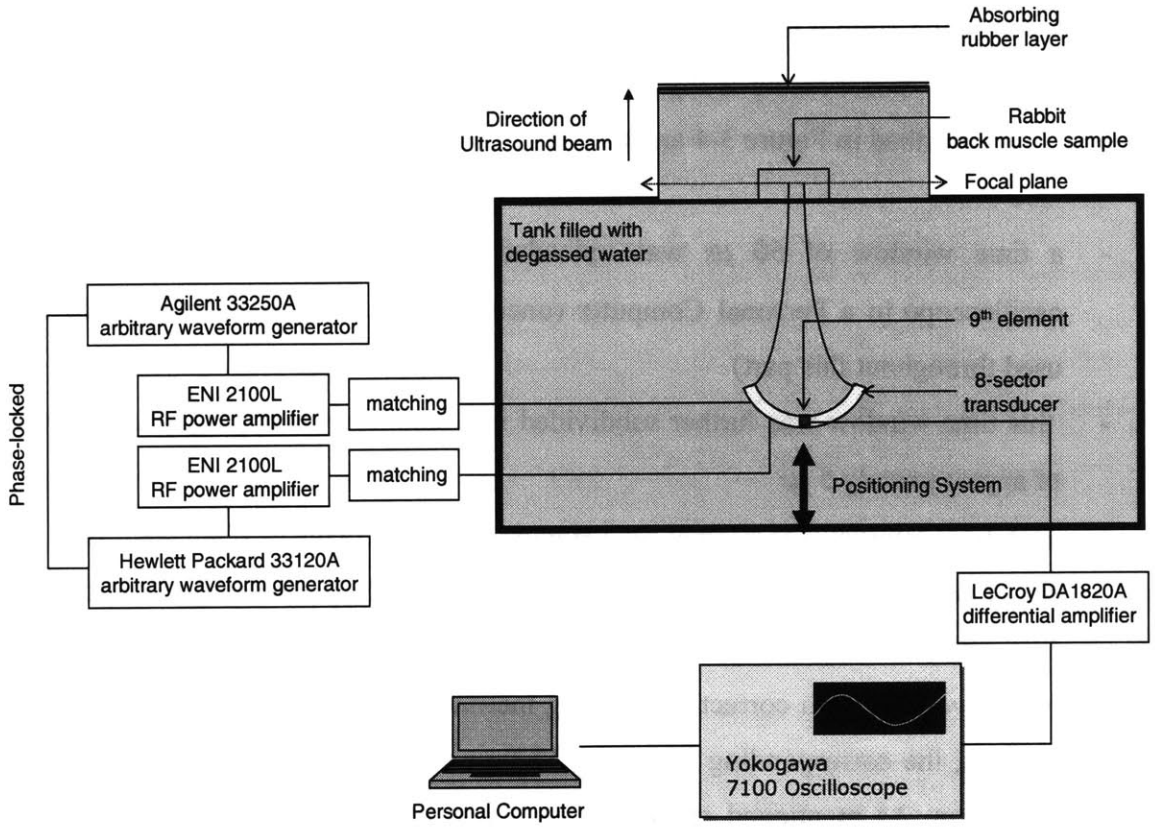

Figure 3-3. *Ex vivo* experimental setup

We first studied the relationship between cavitation threshold and first harmonic phase at a given location in the field. The geometrical focus of the transducer was used. Figure 3-3 shows the experimental setup used to determine relative cavitation threshold in *ex vivo* conditions. A control experiment consisted in replacing the rabbit sample by the same vial filled with degassed water and Optison™ that Sokka *et al* used. The

Optison™ concentration as well as the corresponding experimental protocol was strictly followed. Since the driving voltage is linearly proportional to the driving pressure, we were able to directly measure the cavitation threshold as being the voltage level at which inertial cavitation started.

3.2.4.2. *Ex vivo* experiment: determination of cavitation field

In this section, we present a new method for assessing the cavitation field, that is, in this case, the cavitation threshold along the transducer axis. With the experimental setup described in Figure 3-3, it was impossible to move the rabbit sample along the transducer axis and simply raise the input voltage until inertial cavitation was observed. We then decided to substitute a digital signal processing scheme to this mechanical method. It is described in Figure 3-4 and consists of several steps:

- a time window of 50 μs was uploaded from the Yokogawa 7100 storage oscilloscope to a Personal Computer (once again, a 50-*MHz* sampling rate was used throughout this part)
- this time window was further subdivided into smaller overlapping time intervals of approximately 5 μs
- each time interval was filtered by a Hanning window. This step allowed us to get rid of possible spurious frequency components while performing the upcoming FFT analysis. In practice, we noticed that bypassing this extra filtering step did not prevent us from correctly assessing inertial cavitation activity. For each time interval, the corresponding 256-point FFT was computed and then inspected for cavitation. As mentioned earlier, a broadband noise in the subharmonic region denoted inertial cavitation
- for each time interval, that is, for each depth along the transducer axis, the minimum input voltage at which inertial cavitation occurred was measured. In order to calculate the corresponding cavitation threshold, the minimum input voltage at which inertial cavitation occurred was divided by the relative acoustic pressure at the location of concern. This relative acoustic pressure was determined from hydrophone measurements made earlier in Part *2.2.5*. A relative cavitation

threshold versus depth curve was then computed by dividing every cavitation threshold by the minimum recorded cavitation threshold. Results are presented in Figure 3-8.

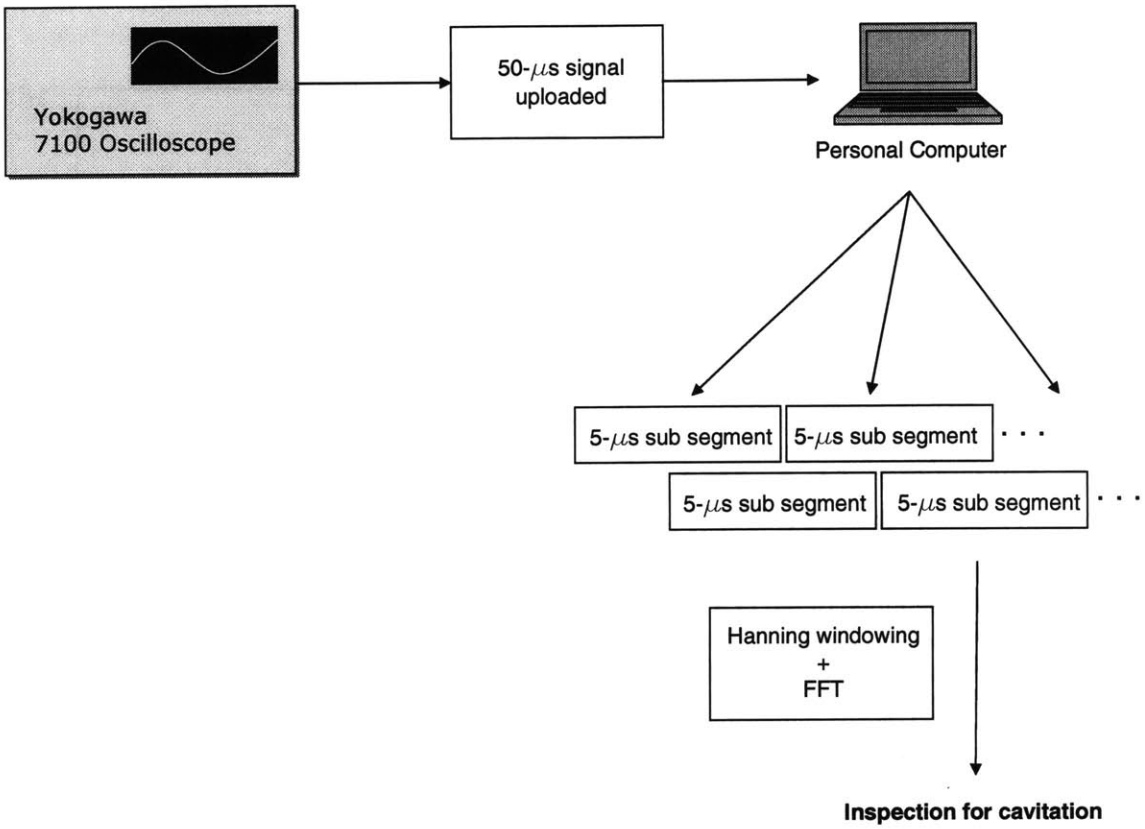

Figure 3-4. Digital signal processing scheme used to measure a cavitation field

The cavitation field which resulted from a sonication characterized by a first harmonic phase angle of 225° was measured. Such a phase angle value was determined to lead to an optimal cavitation threshold differential along the transducer axis, which is a low focal cavitation threshold as compared to near field values. In such conditions, it becomes possible to surpass the cavitation threshold at the focus of the transducer while being sub-threshold in the near field. As a control experiment, we sonicated rabbit back muscle samples with only one of the two aforementioned frequencies. That is all the 8 sectors were sending in phase a 2.4-*MHz* 5-μs burst. The resulting cavitation fields could then be compared and beneficial effects of dual-frequency excitation assessed.

Below is an example of acoustic signals that were processed as explained in Figure 3-4. In figure 3-5(a), the backscattered acoustic signal did not show any sign of inertial cavitation. In figure 3-5(b) though, the backscattered acoustic signal (and more precisely the magnitude of its FFT) exhibited broadband subharmonic emission, which indicates inertial cavitation.

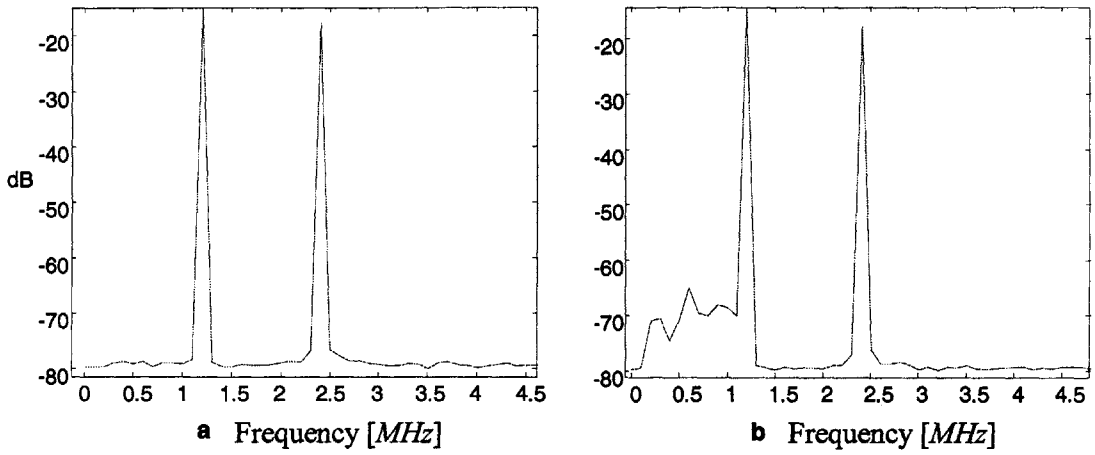

Figure 3-5. (a) Magnitude of the FFT of a backscattered acoustic signal coming from the geometrical focus of the transducer. No inertial cavitation observable. **(b)** Magnitude of the FFT of a backscattered acoustic signal coming from the geometrical focus of the transducer. Inertial cavitation observable

3.3. Results

3.3.1. *Ex vivo* validation of relative cavitation thresholds at the geometrical focus of the therapeutic transducer

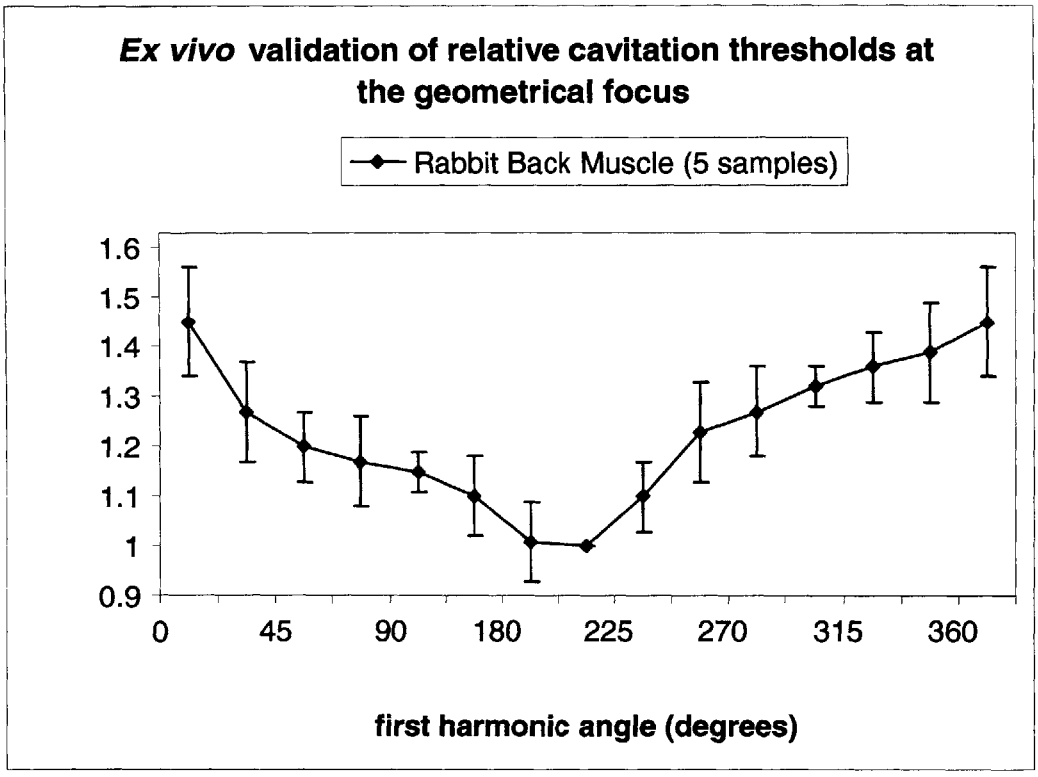

Figure 3-6. *Ex vivo* validation of relative cavitation thresholds at the geometrical focus

Relative cavitation thresholds were measured at the geometrical focus of the therapeutic transducer. They are presented in Figure 3-6. To perform a reliable statistical study, five different rabbit samples were used. The results of the control experiment, which consisted in sonicating a vial filled with a mixture of degassed water and Optison™, are presented in Figure 3-7. By comparing these two plots, we noticed that the general trend is preserved and the cavitation threshold differential is almost the same for both experiments between a phase of 0 and roughly 200°. Such an observation allows us to predict that inertial cavitation seems controllable when the sonication consists of a dual-frequency excitation.

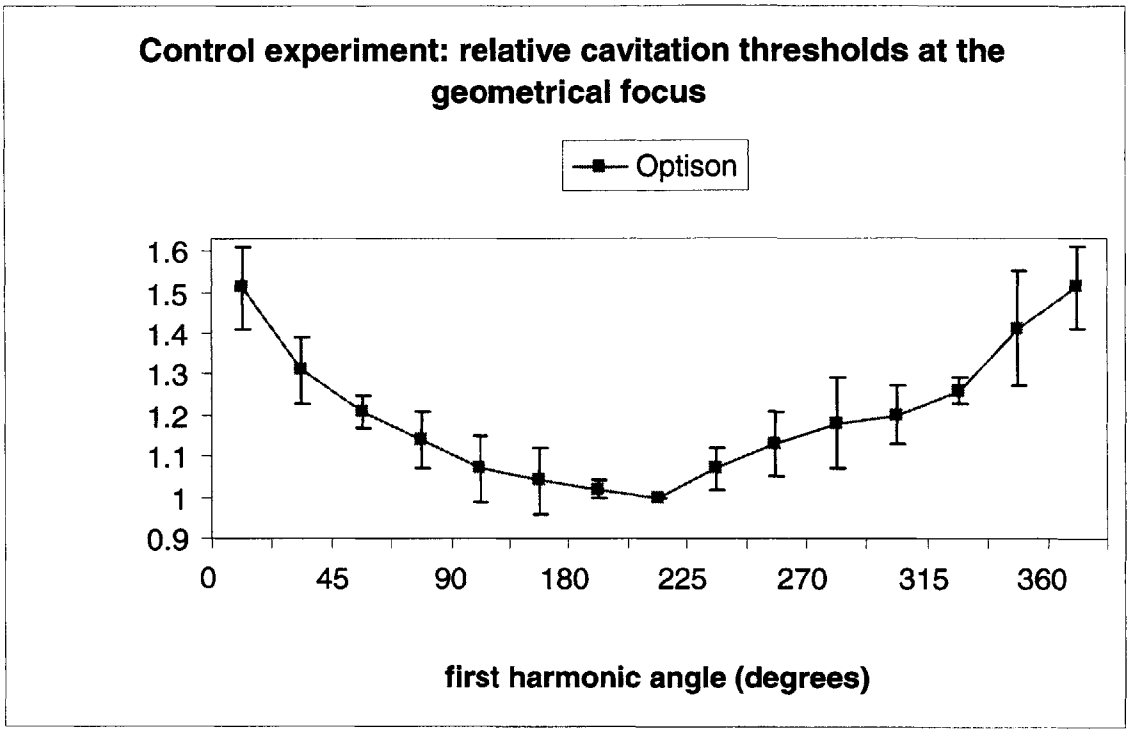

Figure 3-7. Control experiment: relative cavitation thresholds at the geometrical focus

3.3.2. *Ex vivo* validation of cavitation fields

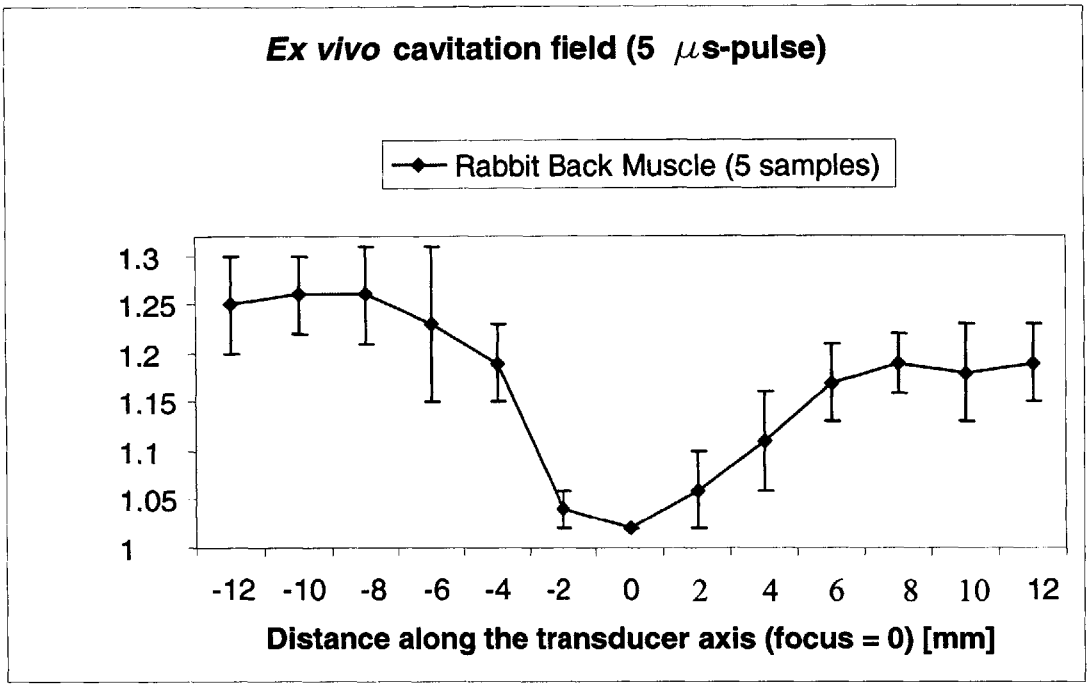

Figure 3-8. *Ex vivo* cavitation field (first harmonic phase angle = 225°)

The cavitation field which resulted from a sonication characterized by a first harmonic phase angle of 225° was thought to be optimal according to simulation results, in the sense that it provides the best near field cavitation suppression while allowing inertial cavitation at the focus. *Ex vivo* cavitation field is presented in Figure 3-8. Since there is not much focused energy in the far field, that is, deeper than the geometrical focus, little attention should be directed towards cavitation threshold values in this region whereas inertial cavitation events in the near field, that is, closer to the transducer surface than the geometrical focus, are more likely to occur as there is more acoustic energy deposited in the propagation medium. Here it is important to notice that dual-frequency excitation manages to lower cavitation threshold in the focal region while the required acoustic pressure to induce inertial cavitation in the near field is raised by 17 % to 25 % of the focal cavitation threshold.

As a conclusion, these *ex vivo* results showed a significant improvement over a single-frequency sonication. When a single-frequency excitation was used, as displayed in Figure 3-9, an essential feature of the dual-frequency situation did not show up. There was

no cavitation threshold bump right before the geometrical focus in the control experiment, which means that the immediate near field was more likely to be stimulated as well. Moreover, in a single-frequency situation, one may expect all points in space to be stimulated with similar waveforms varying only by phase. In the *in vitro* experiments, we observed a virtually constant relative cavitation threshold value along the transducer axis. However, in that situation, microbubbles were sonicated in CW (Continuous Wave) mode. Here, in *ex vivo* experiments, pulses were only 5 μs long and therefore the CW assumption did not apply. As a consequence, timing issues might have come into play and accounted for the non-flat *ex vivo* control cavitation field displayed in Figure 3-9. We noticed that focal relative cavitation threshold was still the lowest in the field but however, the cavitation threshold differential was not as significant as in a dual-frequency situation. On a final note, the determination of this control cavitation field also made use of *in vitro* acoustic pressure measurements as described in Section *2.2.5*. A refinement could consist in taking absorption in tissue into account in order to use more suitable acoustic pressure values.

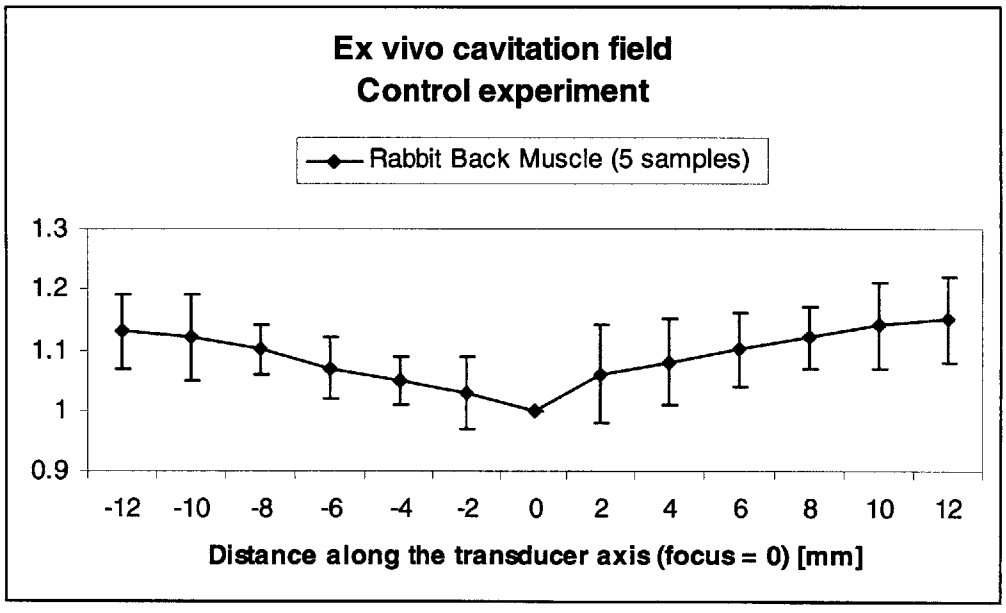

Figure 3-9. *Ex vivo* experimental cavitation field along the transducer. Control experiment (the 8 sectors were sending in phase a 2.4-*MHz* 5-μs burst)

4. Conclusions and recommendations for future work

4.1. Conclusions

Throughout the history of therapeutic ultrasound, there has always been a long-standing debate on relative efficiency of thermal and cavitation based techniques for *in vivo* therapy. Recently, thermal techniques have been used almost exclusively in clinical therapy. This is due to their predictability, controllability, and relative safety. Even if cavitation based ultrasound therapies such as targeted drug delivery and gene therapy might be extensively used in the future, there is still a poor control over bubble activity in tissue. This is primarily because of this lack of control that clinical development of cavitation-based therapies is limited.

The goal of this thesis was to continue a study initiated by Sokka (Sokka 2003a). First, we deepened the analysis of dual-frequency techniques that selectively lower the cavitation threshold at the focus relative to other locations. This consisted in optimizing algorithms developed by Sokka (Sokka 2003a) and checking predictions in *in vitro* conditions. The second half of this thesis consisted in designing and implementing an *ex vivo* experiment which also confirmed theoretical predictions. This part specifically involved the development of signal processing based methods, which were substituted to mechanical methods developed in the first part of this thesis. Moreover, the experimental setup was specifically designed to be MRI-compatible and therefore to allow further *in vivo* investigations.

Results from Chapter *3* of this thesis correlate very well with theoretical predictions and *in vitro* results. Even if we did not use CW mode but a burst mode instead, resulting cavitation fields were very similar to those measured *in vitro*. Moreover, the results from a control experiment which are presented in Figure 3-9 highlighted potentially useful timing effects. Since pulses were only 5-μs long, the CW assumption did not apply. As a consequence, the non-flat *ex vivo* control cavitation field might be accounted for by additional timing effects, which did not come into play in the *in vitro* setup. In other words, when pulses are short enough, they only superimpose perfectly at the geometrical focus of the transducer. Anywhere else in the field, and especially along the transducer axis, this

perfect superimposition does not occur any longer and therefore, less acoustic energy is delivered to those locations. In summary, such a timing effect could potentially enable us to even better control cavitation than by just shaping the acoustic field through the use of dual-frequency waveforms.

4.2. Recommendations for future work

In the first chapter of this thesis, a method to evaluate the cavitation field of an ultrasound transducer with a known excitation pattern was tested experimentally. The technique involved two basic steps: first, the acoustic field for a given transducer with known excitation pattern was either theoretically calculated or experimentally measured. Then the cavitation threshold was calculated in space using the time-domain acoustic field as the input pressure excitation to a bubble model incorporating rectified diffusion. In this study, the Rayleigh-Sommerfeld integral was used to calculate the theoretical acoustic field and the Keller-Miksis bubble model with Flynn's rectified diffusion equation was used to predict cavitation threshold. According to Sokka, these equations combine to provide an excellent first order representation of the cavitation field. However, there are clear limitations to the theory that a sole set of *in vitro* experiments does not necessarily highlight. First, the cavitation field that was calculated assumes a fixed initial bubble radius for the entire field, that is, the seeding bubble size was assumed to be 1 μm throughout the field. In reality, bubbles of various sizes might be present in the field especially if vasculature and tissue interfaces are present. However, trends within one waveform family for various bubble radii showed that the relative cavitation field is relatively invariant to different bubble radii despite the variability of the absolute pressure threshold. In addition, the constant bubble radius assumption is an accurate representation of therapy techniques with injected bubbles as the bubble radii fit a tight distribution. Second, multi-bubble effects as well as the effects of gas saturation were not modeled. Third, our model assumes a homogeneous medium, water, which is clearly not representative of inhomogeneous tissue. However, Keller-Miksis equation has been verified to make reasonable predictions of bubble activity in tissue-mimicking materials for large amplitude ultrasound excitations (Holt and Roy 2001). Lastly, the acoustic wave propagation was assumed to be linear, so phase aberration effects in the field as well as the generation of harmonics were neglected. Despite these limitations, Sokka's model of the cavitation field correlates well with controlled *in vitro* experiments presented in this thesis. Therefore, *in vitro* results may be used to predict the magnitude of the relative cavitation threshold as well as the general trend for one waveform family.

Sokka's model was used to test the cavitation control capabilities of a basic 8-sector transducer. Dual-frequency excitations with this transducer were investigated to develop ultrasound excitation profiles that would preferentially lower the cavitation threshold at the focus relative to other regions in space, specifically the axial nearfield of the transducer. We successfully showed that with this simple phased array, dual-frequency excitations could be used to generate fields where the average cavitation threshold pressure in the nearfield is more than 20 % greater than at the focus. The cavitation field obtained experimentally could be used to tightly control the site of cavitation near tissue interfaces, blood vessels, or fat which might exhibit lower thresholds and induce unwanted cavitation in the nearfield of the transducer.

The experimental results of this first part showed that the threshold of ultrasound induced inertial cavitation could be controlled as a function of space in an ultrasound field. This control would further allow increased targeting beyond the geometric focusing of the beam and may be useful for many clinical applications of focused ultrasound.

Even if the *ex vivo* experiment already incorporates tissue inhomogeneities, there are still relevant factors, which are not taken into account. For example, *ex vivo* conditions do not include perfusion effects. In order to fully characterize and validate dual-frequency methods, several *in vivo* experiments should be carried out. In a first set of experiments, we may want to reproduce plots such as Figure 2-7 and 3-6 to observe cavitation differentials *in vivo*. In a second set of experiments, we may want to correlate subharmonic emission with hot spots on temperature maps obtained with MR imaging. As emphasized by Sokka in his PhD thesis (Sokka 2003a), cavitation activity may generate different temperature spots' shapes; bubble may also act as barrier causing the absence of spots in the far field for example.

Other ways to ensure a proper spatial control of cavitation may also be investigated. In the second part of this thesis, we noticed that when pulses are short enough, timing issues come into play and might be helpful in order to tightly control the cavitation. In such a situation, signals generated from multiple elements only add up perfectly at the

geometrical focus of the transducer and therefore cavitation becomes much likely to occur at the focus while leaving the nearfield inert.

References

Apfel R E 1981 Acoustic cavitation prediction *Journal of the Acoustical Society of America* **69** 6 1624

Atchley A A, Frizzell L A, Apfel R E, Holland C K, Madanshetty S and Roy R A 1988 Thresholds for cavitation produced in water by pulsed ultrasound *Ultrasonics* **26** 5 280-5

Bailey M R, Andew M A, Crum L A and Vaezy S 2002 Dual frequency high intensity focused ultrasound to control bubbles *Proceedings 2nd International Symposium on Therapeutic Ultrasound*

Bush N L, Rivens I, ter Haar G R and Bamber J C 1993 Acoustic properties of lesions generated with an ultrasound therapy system *Ultrasound in Medicine and Biology* **19** 9 789-801

Carstensen E L, Becroft S A, Law W K and Barber D B 1981 Finite amplitude effects on thresholds for lesion production in tissues by unfocused ultrasound *Journal of the Acoustical Society of America* **70** 302-9

Chapelon J Y, Dupenloup F, Cohen H and Lenz P 1996 Reduction of cavitation using pseudorandom signals *IEEE Transactions on Ultrasonics, Ferroelectrics, and Frequency Control* **43** 4 623

Chavrier F, Chapelon J Y, Gelet A and Cathignol D 2000 Modeling of high-intensity focused ultrasound-induced lesions in the presence of cavitation bubbles *Journal of the Acoustical Society of America* **108** 1 432-40

Chung A H, Jolesz F A and Hynynen K 1999 Thermal dosimetry of a focused ultrasound beam *in vivo* by magnetic resonance imaging *Medical Physics* **26** 9 2017-26

Chung A H, Hynynen K, Colucci V, Oshio K, Cline H E and Jolesz F A 1996 Optimization of spoiled gradient-echo phase imaging for *in vivo* localization of a focused ultrasound beam *Magnetic Resonance in Medicine* **36** 5 745-52

Church C C 1988 Prediction of rectified diffusion during nonlinear bubble pulsations at biomedical frequencies *Journal of the Acoustical Society of America* **83** 6 2210-7

Clarke R L and ter Haar G R 1997 Temperature rise recorded during lesion formation by high-intensity focused ultrasound *Ultrasound in Medicine and Biology* **23** 2 299-306

Cline H E, Hynynen K, Watkins R D, Adams W J, Schenck J F, Ettinger R H, Freund W R, Vetro J P and Jolesz F A 1995 Focused ultrasound system for MR imaging-guided tumor ablation *Radiology* **194** 3 731-7

Coakley W T 1971 Acoustical detection of single cavitation events in a focused field in water at 1 MHz *Journal of the Acoustical Society of America* **49** 3 792

Crum L A 1980 Measurements of the growth of air bubbles by rectified diffusion *Journal of the Acoustical Society of America* **68** 1 203-11

Damianou C, Hynynen K and Fan X 1995 Evaluation of accuracy of a theoretical model for predicting the necrosed tissue volume during focused ultrasound surgery *IEEE Transactions on Ultrasonics, Ferroelectrics, and Frequency Control* **42** 182-7

Duck F A 1998 Ultrasound in medicine *Institute of Physics Publishing* Bristol, UK

Edson P L 2001 The role of acoustic cavitation in enhanced ultrasound-induced heating in a tissue-mimicking phantom *PhD thesis* Boston University

Eller A I 1969 Growth of bubbles by rectified diffusion *Journal of the Acoustical Society of America* **46** 5 1246

Eller A I and Flynn H G 1969 Generation of subharmonics of order one-half by bubbles in a sound field *Journal of the Acoustical Society of America* **46** 3 722

Eller A I and Flynn H G 1965 Rectified diffusion through nonlinear pulsations of cavitation bubbles *Journal of the Acoustical Society of America* **37** 493-503

Flynn H G 1982 Generation of transient cavities in liquids by microsecond pulses of ultrasound *Journal of the Acoustical Society of America* **72** 6 1926

Flynn H G 1975 Cavitation dynamics. I. A mathematical formulation in sound field *Journal of the Acoustical Society of America* **58** 6 1160-70

Flynn H G 1964 Physics of acoustic cavitation in liquids *Physical Acoustics* (Mason W P) vol. 1 part B *Academic Press* New York, NY

Fry F J, Sanghvi N T, Foster R S, Bihrle R and Hennige C 1995 Ultrasound and microbubbles: their generation, detection, and potential utilization in tissue and organ therapy – experimental *Ultrasound in Medicine and Biology* **21** 9 1227-37

Fry F J, Kossoff G, Eggleton R C and Dunn F 1970 Threshold ultrasonic dosages for structural changes in the mammalian brain *Journal of the Acoustical Society of America* **48** 6

Fry W J 1954 Production of focal destructive lesions in the central nervous system with ultrasound *Journal of Neurosurgery* **11** 471-8

Fry W J, Wulff V J, Tucker D and Fry F J 1950 Physical factors involved in ultrasound induced changes in living systems: I. Identification of non-temperature effects *Journal of the Acoustical Society of America* **22** 867-71

Gaitan F D, Crum L A, Church C C and Roy R A 1992 Sonoluminescence and bubble dynamics for a single, stable, cavitation bubble *Journal of the Acoustical Society of America* **91** 6 3166

Gilmore F R 1952 Hydrodynamics *Laboratory Report* 26-4 California Institute of Technology

Greenleaf W J, Bolander M E, Sarkar G, Goldring M B and Greenleaf J F 1998 Artificial cavitation nuclei significantly enhance acoustically induced cell transfection *Ultrasound in Medicine and Biology* **24** 4 587

Hazle J D, Diederich C J, Kangasniemi M, Price R E, Olsson L E and Stafford R J 2002 MRI-guided thermal therapy of transplanted tumors in the canine prostate using a directional transurethral ultrasound applicator *Journal of Magnetic Resonance Imaging* **15** 4 409-17

Hill C R, Rivens I, Vaughan M G and ter Haar G R 1994 Lesion development in focused ultrasound surgery: a general model *Ultrasound in Medicine and Biology* **20** 3 259-69

Holland C K and Apfel R E 1989 An improved theory for the prediction of microcavitation thresholds *IEEE Transactions on Ultrasonics, Ferroelectrics, and Frequency Control* **36** 2 204-8

Holt R G and Roy R A 2001 Measurements of bubble-enhanced heating from focused, MHz-frequency ultrasound in a tissue-mimicking material *Ultrasound in Medicine and Biology* **27** 10 1399-412

Hynynen K, McDannold N, Vykhodtseva N and Jolesz F A 2001 Noninvasive MR imaging-guided focal opening of the blood-brain barrier in rabbits *Radiology* **220** 3 640-6

Hynynen K, Colucci V, Chung A and Jolesz F 1996a Non-invasive arterial occlusion using MRI-guided focused ultrasound *Ultrasound in Medicine and Biology* **22** 8 1071-7

Hynynen K, Freund W R, Cline H E, Chung A H, Watkins R D, Vetro J P and Jolesz F A 1996b A clinical noninvasive MRI monitored ultrasound surgery method *RadioGraphics* **16** 1 185-95

Hynynen K, Damianou C, Darkazanli A, Unger E and Schenck J F 1993 The feasibility of using MRI to monitor and guide noninvasive ultrasound surgery *Ultrasound in Medicine and Biology* **19** 1 91-2

Hynynen K 1991 The threshold for thermally significant cavitation in dog's thigh muscle *in vivo Ultrasound in Medicine and Biology* **17** 2 157-69

Hynynen K and Lulu B A 1990 Hyperthermia in cancer treatment *Investigate Radiology* **25** 7 824-34

Ishihara Y, Calderon A, Watanabe H, Mori K, Okamoto K, Suzuki T, Sako K, Kuroda K, Nakagawa N and Tsutsumi S 1995 A precise and fast temperature mapping using water proton chemical shift *Magnetic Resonance in Medicine* **34** 6 814

Johnson C 1972 Nonionizing electromagnetic wave effects in biological materials and system *IEEE Proceedings* **60** 6 692-718

Keller J B and Miksis M 1980 Bubble oscillations of large amplitude *Journal of the Acoustical Society of America* **68** 2 628

Kirkwood J G and Bethe H A 1942 report 558 *Office of Science Research and Development* USA

Lauterborn W 1976 Numerical investigation of nonlinear oscillations of gas bubbles in liquids *Journal of the Acoustical Society of America* **59** 283

Lehmann J F and Herrich J F 1953 Biological reactions to cavitation, a consideration for ultrasound therapy *Arch. Phys. Med. Rehab.* **34** 86-98

Leighton T G 1994 The acoustic bubble *Academic Press* London, UK

Lele P P 1987 Effects of ultrasound on solid mammalian tissues and tumors *in vivo Ultrasound: medical applications, biological effects, and hazard potential* 275-306 (Repacholi M H, Grandolfo M and Rindi A) *Plenum Publishing Corporation* New York, NY

Lele P P 1977 Threshold and mechanisms of ultrasonic damage to organized animal tissues *Proceedings of the Symposium on biological effects and characterization of ultrasound sources* 224-39

Lele P P and Pierce A D 1972 The thermal hypothesis of the mechanism of ultrasonic focal destruction in organized tissues *Interaction of Ultrasound and Biological Tissues.* Rockville, MD: DHEW/FDA 73-8008, 103-7

Lewin P A and Bjorno L 1981 Acoustic pressure amplitude thresholds for rectified diffusion in gaseous microbubbles in biological tissue *Journal of the Acoustical Society of America* **69** 3 846

Lizzi F L and Ostromogilsky M 1987 Analytical modeling of ultrasonically induced tissue heating *Ultrasound in Medicine and Biology* **13** 10 607-18

McDannold N, Hynynen K and Jolesz F 2001 MRI monitoring of the thermal ablation of tissue: effects of long exposure times *Journal of Magnetic Resonance Imaging* **13** 421-7

McDannold N, Hynynen K, Wolf D, Wolf G and Jolesz F A 1998 MRI evaluation of thermal ablation of tumors with focused ultrasound *Journal of Magnetic Resonance Imaging* **8** 1 91-100

Miller D L and Geis R A 1998 The interaction of ultrasonic heating and cavitation in vascular bioeffects on mouse intestine *Ultrasound in Medicine and Biology* **21** 1 123-8

Parlitz U, Englisch V, Scheffczyk C and Lauterborn W 1990 Bifurcation structure of bubble oscillators *Journal of the Acoustical Society of America* **88** 2 1061

Prat F, Chapelon J Y, Fadil A, Sibille A, Theilliere Y, Ponchon T and Cathignol D 1994 Focused liver ablation by cavitation in the rabbit: a potential new method of extracorporeal treatment *Gut* **35** 3 395-400

Prosperetti A, Crum L A and Commander K W 1988 Nonlinear bubble dynamics *Journal of the Acoustical Society of America* **83** 2 502

Samulski T V, Macfall J, Zhang Y, Grant W and Charles C 1992 Non-invasive thermometry using magnetic resonance diffusion imaging: potential for application in hyperthermic oncology *International Journal of Hyperthermia* **8** 6 819-29

Sanghvi N T 1998 Role of cavitation during high intensity focused ultrasound treatment of prostate tissue *Proceedings of the 16th International Congress on Acoustics and the 135th Meeting of the Acoustical Society of America*

Sokka S D 2003a Cavitation methods in therapeutic ultrasound: techniques, mechanisms, and system design *PhD thesis* Massachusetts Institute of Technology

Sokka S D, King R and Hynynen K 2003b MRI-guided gas bubble enhanced ultrasound heating in *in vivo* rabbit thigh *Physics in Medicine and Biology* **48** 223-41

Sokka S D, Juste J and Hynynen K 2003c Design and evaluation of broadband multi-channel ultrasound driving system for large scale therapeutic phased arrays *Proceedings of IEEE Ultrasonics Symposium*

Stepanow B, Huber P, Brix G, Debus J, Bader R, van Kaick G and Lorenz W J 1995 Fast MRI temperature monitoring: application in focused ultrasound therapy of malignant tissue *in vivo SMR 3rd Meeting Proceedings ISSN 1065-9889* 1172

Tran B C, Seo J, Hall T L, Fowlkes J B and Cain C A 2000 Microbubble-enhanced cavitation for non-invasive ultrasound surgery *IEEE Transactions on Ultrasonics, Ferroelectrics, and Frequency Control* **50** 10 1296-304

Umemura S and Kawabata K 1996 Enhancement of sonodynamic tissue damage production by second-harmonic superimposition: theoretical analysis of its mechanism *IEEE Transactions on Ultrasonics, Ferroelectrics, and Frequency Control* **43** 1054-62

Vallancien G, Harouni M, Guillonneau B, Veillon B and Bougaran J 1996 Ablation of superficial bladder tumors with focused extracorporeal pyrotherapy *Urology* **47** 2 204-7

Wu J 1998 Temperature rise generated by ultrasound in the presence of contrast agent *Ultrasound in Medicine and Biology* **24** 2 267-74

Zemanek J 1971 Beam behavior within the nearfield of a vibrating piston *Journal of the Acoustical Society of America* **49** 1 181